Biochimica et Biophysica Acta 1865 (2017) 875–890

Contents lists available at ScienceDirect

Biochimica et Biophysica Acta

journal homepage: www.elsevier.com/locate/bbapap

Evaluation of non-supervised MALDI mass spectrometry imaging combined with microproteomics for glioma grade III classification☆

Emilie Le Rhun [a,b,c,*,1], Marie Duhamel [a,1], Maxence Wisztorski [a], Jean-Pascal Gimeno [d], Fahed Zairi [a,e], Fabienne Escande [f], Nicolas Reyns [e], Firas Kobeissy [g,h], Claude-Alain Maurage [f], Michel Salzet [a], Isabelle Fournier [a,*]

[a] Univ. Lille, INSERM U1192, Laboratoire Protéomique, Réponse Inflammatoire et Spectrométrie de Masse (PRISM), F-59000 Lille, France
[b] Lille University Hospital, Neuro-Oncology, Department of Neurosurgery, F-59000 Lille, France
[c] Breast Unit, Department of Medical Oncology, Oscar Lambret Center, Lille, France
[d] ONCOLille, Maison Régionale de la Recherche Clinique, F-59000 Lille, France
[e] Lille University Hospital, Department of Neurosurgery, F-59000 Lille, France
[f] Lille University Hospital, Pôle Pathologie Biologique, Service Anatomie Pathologique, F-59000 Lille, France
[g] Department of Biochemistry and Molecular Genetics, Faculty of Medicine, American University of Beirut, Lebanon
[h] Department of Psychiatry, Center of Neuroproteomics and Biomarkers Research, University of Florida, Gainesville, FL, USA

ARTICLE INFO

Article history:
Received 26 June 2016
Received in revised form 17 November 2016
Accepted 20 November 2016
Available online 24 November 2016

Keywords:
Anaplastic glioma
WHO classification
Matrix-assisted laser desorption/ionization mass spectrometry imaging
Microproteomics

ABSTRACT

An integrated diagnosis using molecular features is recommended in the 2016 World Health Organization (WHO) classification. Our aim was to explore non-targeted molecular classification using MALDI mass spectrometry imaging (MALDI MSI) associated to microproteomics in order to classify anaplastic glioma by integration of clinical data. We used fresh-frozen tissue sections to perform MALDI MSI of proteins based on their digestion peptides after *in-situ* trypsin digestion of the tissue sections and matrix deposition by micro-spraying. The generated 70 μm spatial resolution image datasets were further processed by individual or global segmentation in order to cluster the tissues according to their molecular protein signature. The clustering gives 3 main distinct groups. Within the tissues the ROIs (regions of interest) defined by these groups were used for microproteomics by micro-extraction of the tryptic peptides after on-tissue enzymatic digestion. More than 2500 proteins including 22 alternative proteins (AltProt) are identified by the Shotgun microproteomics. Statistical analysis on the basis of the label free quantification of the proteins shows a similar classification to the MALDI MSI segmentation into 3 groups. Functional analysis performed on each group reveals sub-networks related to neoplasia for group 1, glioma with inflammation for group 2 and neurogenesis for group 3. This demonstrates the interest on these new non-targeted large molecular data combining both MALDI MSI and microproteomics data, for tumor classification. This analysis provides new insights into grade III glioma organization. This specific information could allow a more accurate classification of the biopsies according to the prognosis and the identification of potential new targeted therapeutic options. This article is part of a Special Issue entitled: MALDI Imaging, edited by Dr. Corinna Henkel and Prof. Peter Hoffmann.

Abbreviations: A, Astrocytoma; ACN, Acetonitrile; ATRX, Alpha-Thalassemia/mental Retardation syndrome X-linked; CDKN2A, Cyclin-Dependent Kinase Inhibitor 2A; CGH-array, Comparative Genomic Hybridization; DNA, Deoxyribonucleic Acid; EGFR, Epidermal Growth Factor Receptor; F, Female; FDR, False Discovery Rate; FFPE, Formalin-Fixed Paraffin-Embedded; gCIMP, CpG Island Methylator Phenotype; HCD, Higher Energy Collision Dissociation; HES, Hematoxylin-Eosin Safran; IDH, Isocitrate Dehydrogenase; LC, Liquid Chromatography; H3F3A, H3 Histone, Family 3A; LESA, Liquid Extraction Surface Analysis; LFQ, Label-Free Quantification; M, Male; MALDI, Matrix-Assisted Laser Desorption/Ionization; MALDI MSI, MALDI Mass Spectrometry Imaging; TOF, Time-of-Flight; MeOH, Methanol; MGMT, O-6-Methylguanine-DNA Methyltransferase; MRI, Magnetic Resonance Imaging; MSI, Mass Spectrometry Imaging; O, Oligodendroglioma; OA, Oligo-Astrocytoma; PSM, Peptide Spectrum Matches; PTEN, Phosphatase and Tensin Homolog; ROI, Region of Interest; RNA, Ribonucleic Acid; SNEA, Subnetwork Enrichment Analysis; TERT, Telomerase Reverse Transcriptase; TFA, Trifluoroacetic Acid; TP53, Tumor Protein P53; WHO, World Health Organization.

☆ This article is part of a Special Issue entitled: MALDI Imaging, edited by Dr. Corinna Henkel and Prof. Peter Hoffmann.

* Correspondence to: I. Fournier, U-1192 Inserm, Laboratoire de Protéomique, Réponse Inflammatoire et Spectrométrie de Masse (PRISM), Université de Lille 1, Cité Scientifique, 59655 Villeneuve d'Ascq Cedex, France.

E-mail addresses: emilie.lerhun@chru-lille.fr (E. Le Rhun), marie.duhamel@etudiant.univ-lille1.fr (M. Duhamel), maxence.wisztorski@univ-lille1.fr (M. Wisztorski), jean-pascal.gimeno@univ-lille1.fr (J.-P. Gimeno), fahed.zairi@chru-lille.fr (F. Zairi), fabienne.escande@chru-lille.fr (F. Escande), nicolas.reyns@chru-lille.fr (N. Reyns), firasko@gmail.com (F. Kobeissy), claude-alain.maurage@chru-lille.fr (C.-A. Maurage), michel.salzet@univ-lille1.fr (M. Salzet), isabelle.fournier@univ-lille1.fr (I. Fournier).

[1] Co-contributing author.

http://dx.doi.org/10.1016/j.bbapap.2016.11.012
1570-9639/

1. Introduction

Histological classification and clinical management of gliomas remain challenging. The World Health Organization (WHO) classification is the standard classification for gliomas and is used to guide clinical management according to the subtypes of tumors. It has been shown that molecular information can improve on the 2007 WHO classification [1]. A highly variable clinical outcome was observed between the same subtypes of gliomas, and a high intra and interobserver discrepancy between pathologists has been noted [2].

A new update of the WHO classification has recently been published [3]. The goal of these classifications is to provide information on the prognosis of patients in a pre-determined subtype of tumors and to guide clinical decisions. The integration of immunohistochemical markers and molecular markers to the standard pathological analysis adds objectivity and permits a better prognostic classification by improving the definition of prognostically distinct subtypes of gliomas [1,4]. In the WHO 2016 classification, grades II or III glioma with a glioblastoma-like profile, include *IDH1/2* wild-type status, frequent gains on 7q and losses on 10q and frequent telomerase reverse transcriptase (TERT) promoter mutations are mostly associated with a glioblastoma, an anaplastic astrocytoma or oligoastrocytoma pathological patterns have usually the worse outcome [1]. Thus, the determination of the presence of a +7q/−10q in patients with *IDH1/2* wild-type WHO grade II and III gliomas is relevant [1]. Tumors with an *IDH1/2* mutation, a 1p/19q codeletion, and an oligodendroglial histological subtype have the best prognosis [1,5,6]. Most of these tumors show a proneural glioblastoma-like expression profile, associated with a better outcome [1,7,8]. Yet *IDH1/2* mutation/CpG island methylator phenotype (gCIMP), 1p/19q co-deletion represents the main molecular features required for a better classification of gliomas [1,2,7,8]. Other biological markers of interest are often added, such as *TERT* promoter mutations, gain on chromosome arm 7q (+7q), loss on chromosome arm 10q (−10q), tumor protein p53 (*TP53*), alpha-thalassemia/mental retardation syndrome X-linked (*ATRX*) gene mutations, phosphatase and tensin homolog (PTEN), and Notch pathway gene mutations or (H3 Histone, Family 3A) H3F3A and BRAF mutations [1,9–20]. However, their implications and their relevance in refining prognostic information for grade II and grade III gliomas remain to be confirmed [1].

Immunohistochemistry and molecular-based classification of glioma have improved the determination of the prognosis and integrated diagnosis should now be required as part of tumor assessment in the clinical practice and help to guide the therapeutic decisions [17,18,21,22]. However, genomic approaches are limited, as some normal, upregulated or mutated genes may not be transcribed [23] and discrepancies have been identified between m-ribonucleic acid (mRNA) and proteomics expression profiles in gliomas [24,25]. The addition of proteomics findings could lead to the discovery of new prognostic information and a better characterization of tumor subtypes, improving thus the clinical decision making. Over the past years, technological advances have been realized in proteomics analysis. The proteomics approach gives access to many proteins' identification, relative quantification, and determination of post-translational modifications and could also help to identify personalized clinical strategies by determining specific molecular pathways and cellular functions [24,26–30].

In the present study, we aim to investigate glioma grade III molecular features and classification of patients by a non-targeted molecular approach using MALDI MS imaging (MALDI MSI) and spatially-resolved microproteomics. This is achieved by performing MALDI MSI of trypsin digested proteins [31] to retrieve protein distribution within tissues of patients with anaplastic glioma and further non-supervised spatial segmentation of the molecular data [32]. From such classification, regions of interest (ROIs) are selected for the spatially-resolved Shotgun proteomics [33,34]. Comparison between proteomics and histological data is investigated to search for concordance or discordance.

2. Materials and methods

2.1. Patient samples and consent

Samples were prospectively collected from histologically confirmed anaplastic glioma patients recruited between September 2014 and July 2015 at Lille University Hospital, France according to the gliomic study (NCT 02473484). The study adhered to the principles of the Declaration of Helsinki and the Guidelines for Good Clinical Practice. All patients gave written informed consent before enrollment. Patients enrolled in this cohort all had a newly diagnosed anaplastic glioma according to the WHO classification of the central nervous system [3] after pathological examination by the same pathologist (CAM) under routine practice conditions. Other criteria for inclusion included an age of 18 years or more, the absence of other prior cancer or cancer treatment, and the absence of genetic disease potentially leading to cancer. Tumor samples were processed within 2 h after sample extraction in the surgery room to limit the risk of protein degradation.

2.2. Glioma tissue samples for immunohistochemistry and molecular analyses

2.2.1. Immunohistochemistry analyses

IDH1-R132H mutations, ATRX, protein 53 (P53) and epidermal growth factor receptor (EGFR) statuses were determined by immunohistochemistry on formalin-fixed paraffin-embedded (FFPE) tumor tissue samples. 4 μm sections were labeled in an Ultra automate (Ventana-Roche Tissue Diagnostics, Tucson AZ), after antigen retrieval procedures (ATRX, IDH1, and P53: citrate pH 6.0; EGFR: proteinase 2), according to the suppliers' protocols. A punch of positive control tumor was stained on the same slide for IDH1 labeling (tumor tissue from an IDH1 R132H mutated, non-codeleted, astrocytoma). ATRX was determined as positive when cases with more than 10% positive tumor cells were scored positive (ATRX expression). P53 was considered expressed when 10% or more nuclei were deeply stained; EGFR expression was semi-quantified according to Hirsch score, allowed by comparison to the multiscale control. A multiscale positive control was stained in the same series for EGFR labeling. IDH1 R132H was explored using Diavona clone H09, mouse monoclonal at 1/40 dilution, ATRX using Sigma, ref HPA001906 Rabbit polyclonal, at 1/200 dilution, P53 using Dako, clone DO-7, mouse monoclonal, at 1/100 dilution, and EGFR using Invitrogen, clone 31G7, mouse monoclonal, at 1/20 dilution.

2.2.2. Deoxyribonucleic acid (DNA) extraction and quantification

Molecular analyses were performed on FFPE tissues. The following tests were performed: comparative genomic hybridization (CGH)-array, O-6-methylguanine-DNA methyltransferase (MGMT) promoter methylation and IDH1/IDH2 mutations. All tissues used for DNA extraction were histologically evaluated to determine the tumor cell content. Only tissue samples with a minimum tumor cell content of 70% or more were analyzed. DNA extraction from FFPE was performed using the kit QIAamp DNA FFPE Tissue (Qiagen). CGH profiles were determined using a SurePrint G3 Human CGH Microarray Kit, 8x60K (Aligent) and the CytoGenomics v2.7 software. The limit of the resolution was 1 Mb. The presence of 1p/19q codeletion, gain of chromosome 7, loss of chromosome 10, amplification of the EGFR gene and homozygous deletion of the Cyclin-Dependent Kinase Inhibitor 2A (CDKN2A) gene has been systematically evaluated. Mutations affecting codon 132 of *IHD1* (ref seq NM_005896.2), codon 172 of IDH2 (ref seq NM_ 002168.2) were validated by PCR-sequence Sanger when immunohistochemistry was negative. The MGMT promoter methylation status (CpGs 74–78) was determined after bisulfite treatment by pyrosequencing on a PyroMark Q96 with an MGMT PyroMark kit (Qiagen). The presence of methylation was scored as positive when a minimum of 8% of methylation was observed.

2.3. MALDI mass spectrometry imaging (MALDI MSI)

2.3.1. Tissue preparation and image acquisition

A complete experimental workflow of the MALDI MSI combined with microproteomics is described in Fig. 1. Twelve micrometer sections were cut using a cryostat (Leica Microsystems, Nanterre, France) to perform tryptic peptide MALDI MSI analysis. These tissue sections were deposited on ITO-coated glass slides (BrukerDaltonics, Bremem, Germany) and dried for 15 min in a desiccator. Several washes were performed to remove as many abundant lipids as possible: (1) 1 min in 70% ethanol, (2) 1 min in 100% ethanol, (3) 1 min in acetone and (4) 30 s in chloroform. These two last steps were repeated twice. The tissue was dried between each washing step in a desiccator. Trypsin (60 μg/mL, dissolved in NH_4HCO_3 50 mM) was then micro-sprayed on the tissue surface using an electrospray nebulizer attached to a 500 μL syringe at a flow rate of 180 nL/min. The nebulizer was moved uniformly throughout the tissue surface for 15 min. Incubation was performed using ImagePrep (Bruker Daltonics, Bremen, Germany) by microspraying water heated at 37 °C for 2 h. The digestion procedure includes 60 cycles, each cycle corresponding to 2 s spraying, 180 s incubation and 60 s drying using the nitrogen flow of the instrument. During the entire procedure the Imaprep tank was filled with water at 95 °C to maintain a constant humidity atmosphere for digestion improvement. This water as well as the 37 °C water used for spraying was replaced every 30 min during the 2 h of total digestion procedure. Once digestion was over, matrix deposition was performed using ImagePrep. The used matrix was the solid ionic matrix HCCA/ANI [35]. HCCA/ANI is prepared just before use by an acido/basic reaction between the conventional HCCA matrix and the organic base aniline in a ratio equivalent to 1:1. Briefly, 36 μL of aniline were added to 5 mL of a solution of 10 mg/mL HCCA dissolved in ACN/0.1% TFA aqueous (7:3, *v*/*v*). The formation of the organic salt is obtained after a few minutes sonication of the solution. This solution was then loaded into the Imageprep. Uniform deposition of the matrix on the tissue was ensured by careful control of the deposition parameters by monitoring scattered light in real-time during the entire process through the optical sensor equipping the instrument. A method specially developed for the HCCA/ANI matrix was used. This method includes 3 steps of spraying cycles with optimized parameters. Briefly, step 1 comprises 5 cycles at 0.1 V with 1 s spraying, 10 s incubation and 180 s drying. Step 2 includes 8 cycles at 0.2 V including 1.25 s spraying, 30 s incubation and 120 s drying. In step 3, 37 cycles at 0.3 V were performed with 1.55 s spraying, 20 s incubation and drying monitored according to sensor control (25%). Finally, 3 cycles were realized on step 3 with 2 s spray, 20 s incubation and 2/3 drying according to sensor control (25%) and 1/3 allowed to complete drying. After HCCA/ANI deposition, the slides were directly transferred to the MS instrument. MALDI MSI data were acquired on an Ultraflex II MALDI-TOF/TOF instrument (Bruker Daltonics, Bremen, Germany) upgraded with a smartbeam II solid state laser operating up to 200 Hz repetition rate. Mass spectra were acquired in the positive delayed extraction reflectron mode using the 800–4000 *m*/*z* range. Recorded spectra were averaged from 400 laser shots per pixel. MALDI MSI data was acquired using a 70 μm spatial resolution raster.

2.3.2. MALDI MSI data processing and analysis

SCiLS Lab (SCiLS Lab 2015b, SCiLS GmbH) software was used for unsupervised spatial segmentation of anaplastic glioma. MALDI MSI raw data were first imported into SCiLS Lab [36]. Data analysis starts with a preprocessing step of baseline removal using an iterative convolution with sigma 20. A peak picking was realized with a step of alignment and a normalization according to the Total Ion Count applied to every 16th spectrum selecting 100 peaks per spectrum. Afterward, edge-preserving image denoising was carried out using weak filtering. The resulting denoised data were spatially segmented using the bisecting k means algorithm. Different spatial segmentations were performed. First, each tissue (individual segmentation) were segmented separately. Then all the

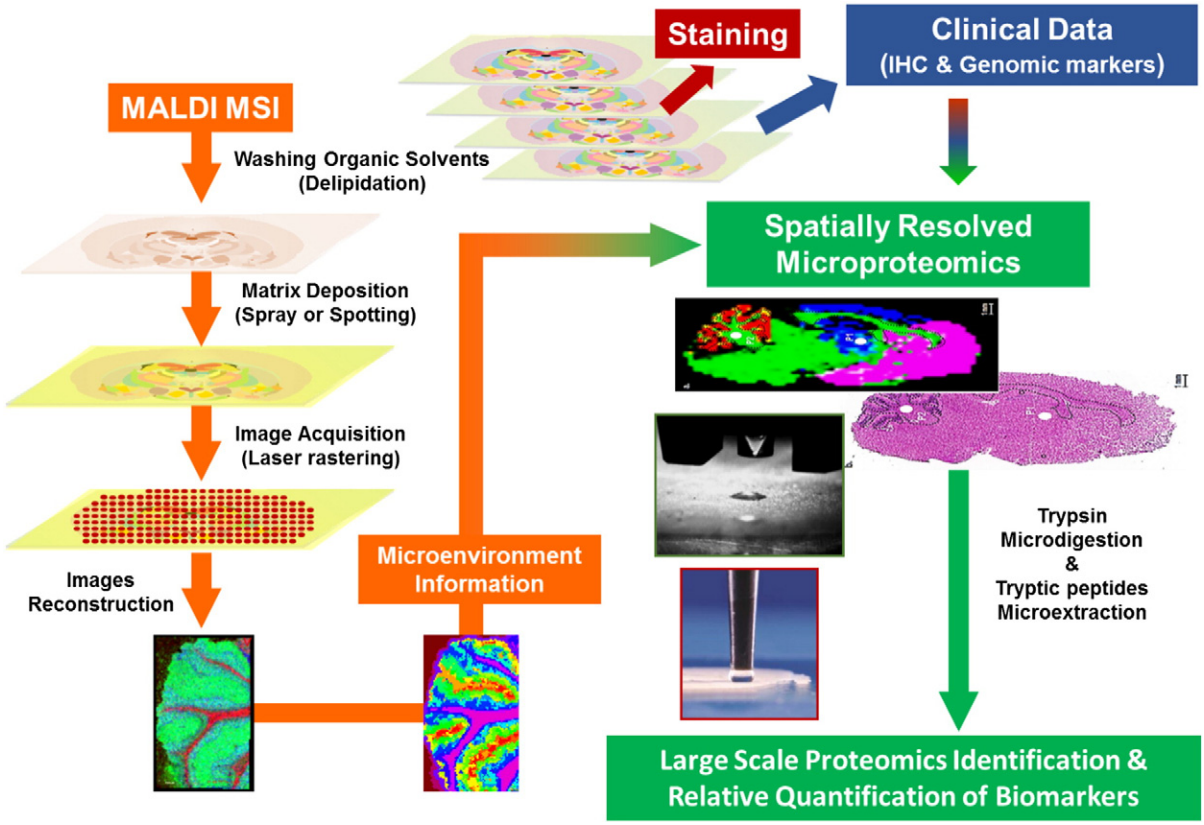

Fig. 1. General workflow of the MALDI-MS imaging combined with microproteomics used for glioma classification.

tissues (global segmentation) were segmented together. Briefly, the segmentation algorithm groups spectra according to the similarity of data after extraction of features. Results of segmentations were represented on a dendrogram, with each branch representing a group of spectra for which a color was attributed to be localized on the resulting molecular image. This gives a segmentation map where regions of distinct molecular composition were color-coded according to the dendrogram. For this step, five samples were submitted to an individual or a global segmentation. A detailed description of this pipeline can be found in reference [37]. For each region, images of specific mass-to-charge (m/z) ratio of ions were reconstructed. The global spatial segmentation allowed us to determine regions of interest (ROIs). These identified ROIs can then be subjected to on-tissue microdigestion followed by microextraction for protein identifications.

A classification model was then generated. The first five patients were used as a training group, and five new patients were included as a test group. For the training, three regions were selected in the clusters defined by the spatial segmentation (blue group, brown group, and green/orange group) to establish the classification model. The validation of the model was done using two different regions in each group. Then the generated model was blind tested with the test group.

2.4. Tissue Shotgun microproteomics

2.4.1. On-tissue LysC-Tryptic microdigestion on tissue

Spatially-resolved microproteomics were realized on the ROIs according to the previously published protocol [34]. Briefly, 20-μm sections were cut using a cryostat (Leica Microsystems, Nanterre, France) and subjected to protein microdigestion. These tissue sections were deposited on poly-lysine glass slides and dried for 15 min in a desiccator. Several washes were performed to remove lipids: (1) 1 min in 70% ethanol, (2) 1 min in 100% ethanol, (3) 1 min in acetone and (4) 30 s in chloroform. These two last steps were repeated twice. The tissue was dried between each step of washing in a desiccator. Then, the LysC-trypsin solution (40 μg/mL, diluted in Tris-HCl 50 mM, pH 8.0) was deposited using the piezoelectric microspotter Chemikal Inkjet Printer (CHIP-1000, Shimadzu, CO, Kyoto, Japan). The digestion was performed on a total area of 1 mm^2 made out of a 4 × 4 pitch of micro-spots. Each spot is 200 μm in diameter and corresponds to a droplet volume of 100 pL/cycle. Enzyme was spotted for 30 min in a row and then changed. This was repeated 4 times for a total of 2 h digestion. After enzyme deposition 0.1%TFA was spotted for 25 cycles with 100 pL on each spot/cycle.

2.4.2. Microextraction by liquid microjunction

After the microdigestion, the peptides within selected regions of tissue sections (ROIs) were extracted using the TriVersa Nanomate platform (Advion Biosciences Inc., Ithaca, NY, USA) with a Liquid Extraction Surface Analysis (LESA) option. Briefly, a volume of solvent was aspirated and deposited onto the digested region and then aspirated again to be dispensed into a low binding tube. Three steps per extraction were done: (1) 0.1% TFA, (2) ACN/0.1% TFA (8:2, v/v), and (3) MeOH: 0.1% TFA (7:3, v/v). Two extractions per point were performed to increase the quantity of material collected.

2.4.3. NanoLC-MS & MS/MS analysis

After liquid microjunction extraction, collected samples were dried under vacuum, reconstituted with 20 μL of 0.1% TFA solution and subjected to desalting using C-18 Ziptip (Millipore, Saint-Quentin-en-Yvelines, France) eluted by 60% ACN and dried under vacuum. Dried samples were reconstituted in 0.1% FA aqueous/ACN (98:2, v/v). The samples were separated by online reversed-phase chromatography using a Thermo Scientific Proxeon Easy nLC 1000 system equipped with a Proxeon trap column (100 μm ID × 2 cm, Thermo Scientific) and a C18 packed-tip column (75 μm ID × 50 cm, Thermo Scientific). Separation was achieved using an increased amount of acetonitrile (5–35% over 100 min) at a flow rate of 300 nL/min. Data were acquired on a Thermo Scientific Q-Exactive mass spectrometer set to acquire the top 10 MSMS in data-dependent mode. The survey scans were done at a resolving power of 70,000 FWHM (m/z 400), in positive mode and using an AGC target of 3e + 6. Default charge state was set at 2, unassigned and +1 charge states were rejected and dynamic exclusion was enabled for 25 s. The scan range was set to 300–1600 m/z. For $ddMS^2$, the scan range was between 200 and 2000 m/z, 1 microscan was acquired at 17,500 FWHM with an isolation window of 4.0 m/z and a HCD Normalized Collision Energy (NCE) of 30 was used.

2.4.4. Data analysis

All MS data were processed with MaxQuant [38,39] (Version 1.5.3.30) using the Andromeda [40] search engine. The proteins were identified by searching MS and MS/MS data against of the complete proteome for *Homo sapiens* in the UniProt database [41] (release February 2016, 70,615 entries) combined with 262 commonly detected contaminants. A second search was also done combining the Human database with an AltORF database previously published [42]. Trypsin specificity was used for digestion mode, with N-terminal acetylation and methionine oxidation selected as variable. We allowed up to two missed cleavages. An initial mass accuracy of 6 ppm was selected for MS spectra, and the MS/MS tolerance was set to 20 ppm for the HCD data. FDR at the peptide spectrum matches (PSM) and protein level was estimated using a decoy version of the previously defined databases (reverse construction) and set to 1%. Relative, label-free quantification of the proteins was conducted into Max-Quant using the MaxLFQ algorithm [43] with default parameters. The data sets and Perseus result files used for analysis were deposited at the ProteomeXchange Consortium [44] (http://proteomecentral.proteomexchange.org) *via* the PRIDE partner repository [44] with the data set identifier PXD004437 (for reviewer access only, Username: reviewer85761@ebi.ac.uk; Password: VgKBKrC2). Analysis of the identified proteins was performed using Perseus software (http://www.perseus-framework.org/) (version 1.5.0.31). The file containing the information from the identification were used and hits from the reverse database, proteins with only modified peptides and potential contaminants were removed. The LFQ intensity was logarithmized (base 2 logarithm). Statistical multiple-sample tests were performed using ANOVA with a truncation value based on "permutation-based FDR" of 5%. Two categorical annotation rows that were used for ANOVA are (1) the group (Group 1, Group 2, Group 3) and (2) the patients (case 1, case 2, case 3, case 4 and case 5). To evaluate the enrichment of the categorical annotations (Gene Ontology terms and KEGG pathway), Fisher's exact test was performed taking into account the results of the ANOVA for each group. Normalization was achieved using a Z-score with matrix access by rows. In Z-score normalization, the mean of each row/column is subtracted from each value. The result is then divided by the standard deviation of the raw/column. Only proteins that were significant by ANOVA were used. Hierarchical clustering was first performed using the Euclidean parameter for the distance calculation, and the average option for linkage in the rows and columns of the trees with a maximum of 300 clusters. Functional annotation and characterization of the identified proteins were performed using PANTHER software (version 9.0, http://www.pantherdb.org) and STRING (version 9.1, www.string-db.org) [45] by uploading the protein list exported from Perseus and corresponding to the overexpressed proteins for each group (Supplementary Tables 1 & 2). STRING is a database containing information about protein-protein interactions. It includes the known or predicted association through five main sources (Genomic Context Predictions, High-Throughput lab experiments, Co-expression, Automated textmining and previous knowledge in database). The algorithm will determine physical or functional associations between proteins of a list and a network of predicted associations could be visualized.

2.4.5. Subnetwork enrichment pathway analyses and statistical testing

The Elsevier's Pathway Studio version 10.0 (Ariadne Genomics/Elsevier) was used to deduce relationships between differentially expressed proteomics protein candidates using the Ariadne ResNet database [46,47]. "Subnetwork Enrichment Analysis" (SNEA) algorithm was selected to extract statistically significant altered biological and functional pathways pertaining to each identified set of protein hits among the different groups. SNEA utilizes Fisher's exact test set to determine if there are nonrandom associations between two categorical variables organized by a specific relationship. Integrated Venn diagram analysis was performed using "the InteractiVenn": a web-based tool for the analysis of complex datasets [48]. InteractiVenn is a tool for interacting with Venn diagrams including up to six sets. It is an interface for Venn diagram construction which enables analysis of set unions while preserving the shape of the diagram. Set unions are useful to reveal differences and similarities among datasets and is guided by a tree or by a list of set unions. See Supp. Tables 3, 4 and 5 as supplementary data for the listed differential pathways

3. Results

3.1. Clinical, pathological and molecular description

Five patients were first analyzed. The median age was 36 years (minimum 27, maximum 69), and 3 patients were male. No necrotic aspect was observed on brain MRI, but contrast enhancement was present in all tumors. Tumors included 2 oligoastrocytomas, 2 astrocytomas and 1 oligodendroglioma. IDH1 mutations were observed in 4 samples, 1p/19q codeletion in 2 samples, ATRX was expressed in 2 samples, P53 was noted in 2 tumors, EGFR in 3 tumors with a median Hirsch score of 200 (range, minimum 120, maximum 350), and a methylated MGMT promoter was found in 5 samples, with a median percentage of methylation of 32% (range, minimum 14.6%, maximum 64.8%). Combined 7 gain and 10 losses was observed in 1 sample. Initial treatment included surgery (complete resections in 1 case, subtotal resection in 3 cases and partial resection in 1 case), followed by radiation therapy in two cases, by radiation therapy then 6 cycles of temozolomide in one case and by radiation therapy and concomitant/maintenance temozolomide in two cases). Median follow-up time was 14.5 months (range, minimum 9 months, and maximum 19.5 months). Two patients among the 5 analyzed presented with a progression (patients 1 and 3). Only one patient died of disease progression 14.4 months after initial diagnosis after two more lines of treatment for recurrent disease (patient 3). This patient had an IDH1 wild-type and non 1p/19q codeleted tumor. The clinical characteristics and the results of the pathological and molecular analysis are presented in Table 1.

Five other patients were then analyzed as a blind test cohort. The median age was 40 years (minimum 30, maximum 60), and 4 patients were male. As for cases, no necrotic aspect was observed on brain MRI, but contrast enhancement was present in all tumors. Tumors included 2 oligodendrogliomas, 2 astrocytomas and 1 oligoastrocytoma. IDH1 mutations were observed in all the 5 samples, 1p/19q codeletion in only 1 sample, ATRX was expressed in 1 sample, P53 was noted in 3 tumors, EGFR in 5 tumors with a median Hirsch score of 200 (range, minimum 110, maximum 300), and a methylated MGMT promoter was found in 4 samples, with a median percentage of methylation of 23% (range, minimum 13.8%, maximum 47.8%). No combined 7 gain and 10 loss was observed. Initial treatment included surgery (complete resections in 4 cases and subtotal in 1 case), followed by radiation therapy in two cases, by radiation therapy then 6 cycles of temozolomide in one case and by radiation therapy and concomitant/maintenance temozolomide in four cases. Median follow-up time was 12.5 months (range, minimum 8 months, and maximum 35 months). No progression was observed during the follow-up, and all patients are still alive. The clinical characteristics and the results of the pathological and molecular analysis are also reported in Table 1 (blind test cohort).

3.2. Histological and molecular studies of the 5 tissue samples in the training cohort

After hematoxylin eosin safran (HES) staining, tissue samples were annotated by the pathologist (Fig. 2A). Necrosis, parenchyma infiltrated by tumor cells, and tumor tissues have been delimited by the pathologist (CAM) in each sample before subjected to MALDI MSI analyses. Cases 1 and 3 presented large tumor areas and small necrosis parts whereas in Case 2, necrosis constituted the main part of the tissue sample. Cases 4 and 5 were homogeneous tumor tissues (Fig. 2A).

The MALDI-MS images were generated from trypsin digested tissue sections, thus monitoring proteins through their tryptic peptides. From the raw MALDI MSI data obtained from each tissue sample, individual clustering was then realized (Fig. 2B) by subjecting resulting spectra of each tissue sample to spatial segmentation. This allows finding out the regions of specific molecular profiles within the tissues. The segmentation map clearly shows discrepancies between classical pathological annotations based on morphological criteria and molecular histology realized by MALDI MSI for 3 tissues. In case number 1, three regions of interest (ROIs) are well delimited on the segmentation map in accordance with the pathological annotations (Fig. 2B). For case number 2, molecular clustering and pathological annotations revealed mainly the presence of 3 different ROIs that could be linked with the morphological annotation of the pathologist. However, a fourth ROI is observed with MSI imaging in the necrotic part, sharing molecular characteristics of the region identified as parenchyma region by the pathologist (Fig. 2B). In case number 3, four ROIs are delimited thanks to MSI imaging while the pathologist only identified two distinct regions. For cases number 4 & 5, the pathologist defined tissue samples as homogeneous tumors, but the MSI data tends to demonstrate that the tissues are more heterogeneous than expected (Fig. 2B).

Individual analyses confirmed the presence of specific ions delimiting these regions (Fig. 2C). In case number 1, the ion at m/z 1952.01 is specific to the tumor region as designed by the pathologist whereas the ion at m/z 1428.17 is specific to the necrosis part. On the other side, ions at m/z 2430.95 and 2608.94 are present in both regions (Fig. 2C). For case number 2, the m/z 1148.94 ion is specific to the infiltrated parenchyma; when m/z 2043.54 is absent from the infiltrated parenchyma and more are present in the tumor and necrotic regions as well as m/z 1686.27 and 1920.71 (Fig. 2C). For case number 3, m/z 1149.95 and 1510.72 are specific to the tumor region (Fig. 2C). In cases number 4 and 5, considered as homogeneous tumors, two regions are identified. These two regions present specific molecular profiles characterized by ions at m/z 1217.92 and 1307.04 for case number 4 and ions at m/z 1499.25 and 1605.44 for case number 5 (Fig. 2C).

Based on these data, we decided to perform a spatial segmentation of the entire set of samples together to compare them to each other and determine if common features can be found among the different cases (Fig. 2D). Global segmentation shows that different cases share common molecular features. Indeed, cases number 1 & 4 presented the same molecular similarities and are grouped together (blue node). Green and orange regions are grouped together for future comparisons with the microproteomics studies. Case number 5 and parts of cases number 2 and 3 belong to the green/orange region. The brown region is on a distinct node and comprises parts of cases number 2 and 3 (Fig. 2D).

3.3. Tissue microproteomics, protein identification and classification

From these global segmentation results, we could thus identify three molecularly different groups among the grade III tissue samples (Fig. 2D). In order to identify the proteins related to each group and in each region of the tissues defined from the MALDI MSI data, we performed microproteomics. For each sample, microextractions were achieved after *in-situ* on-tissue digestion. For cases number 1, 2, 3 and 5, three different microextractions were performed per tissue (see Fig. 1D, 1.1, 1.2

Table 1
Clinical characteristics, pathological and molecular data of the patients.

Cases	Sex	Age at diagnosis	Topography	Necrosis on MRI	Contrast enhancement on MRI	First progression	Death	Histological type	WHO grade	IDH1	1p/19q codeletion	ATRX	P53	EGFR (Hirsch score)	MGMTp status (%)	Chromosomes 7 and 10
Classification cohort																
1	M	69	Fronto-temporo-parietal, left	No	Yes	Yes	No	Oa	3	Positive	No codeletion	Loss	Positive	Positive (220)	Methylated (64.8%)	7p gain, 10p gain
2	M	27	Parietal, right	No	Yes	No	No	Oa	3	Positive	Codeletion	Expressed	Negative	Negative (200)	Methylated (14.6%)	No abnormalities
3	F	45	Frontal, right	No	Yes	No	No	O	3	Positive	Codeletion	Expressed	Negative	Positive (170)	Methylated (32%)	7 gain, 10 loss
4	F	24	Temporo insular, right	No	Yes	Yes	Yes	A	3	Negative	No codeletion	Loss	Positive	Negative (120)	Methylated (16%)	No abnormalities
5	M	45	Frontal, left	No	Yes	No	No	A	3	Positive	No codeletion	Loss	Negative	Positive (350)	Methylated (58%)	No abnormalities
Blind test cohort																
6	M	30	Frontal, right	No	Yes	No	No	O	3	Mutant[a]	No codeletion	Loss	Negative	Positive (200)	Non methylated (2.4%)	7 gain
7	M	40	Frontal, left	No	Yes	No	No	Oa	3	Positive	No codeletion	Loss	Positive	Positive (200)	Methylated (14%)	No abnormalities
8	M	35	Temporal, right	No	Yes	No	No	A	3	Positive	No codeletion	Loss	Positive	Positive (110)	Methylated (16.2%)	7 loss
9	F	54	Frontal, right	No	Yes	No	No	O	3	Positive	Codeletion	Expressed	Negative	Positive (300)	Methylated (47.8%)	No abnormalities
10	M	60	Parietal, right	No	Yes	No	No	A	3	Positive	No codeletion	Loss	Positive	Positive (130)	Methylated (13.8%)	7p gain, 10p gain

Abbreviations:
M: male, F: female, MRI: magnetic resonance imaging, OA: oligo-astrocytoma, A: astrocytoma, O: oligodendroglioma, WHO: World Health Organization, IDH1 ATRX: alpha-thalassemia/mental retardation syndrome X-linked, P53 MGMTp: MGMT promoter.

[a] For this case, IDH R132H was negative, however, the molecular analysis confirmed the presence of IDH1 mutation.

and 1.3, 5.1, 5.2, and 5.3, 22.1, 22.2 and 22.3, 20.1, 20.2 and 20.3 respectively). For case number 4, two microextractions were realized and referenced as 6.1 and 6.2. After extractions, each of the 14 extraction spots were submitted to Shotgun analyses. Proteins with an abundance that was significantly different among the samples were determined according to the MaxQuant and Perseus software. Heat maps were generated from the proteins found to be significant according to ANOVA test using a significance threshold of $P < 0.05$ (Fig. 3A). More than 2500 proteins were identified combining all analyses (Suppl. Table 1). Hierarchical clustering revealed two main branches, separating cases

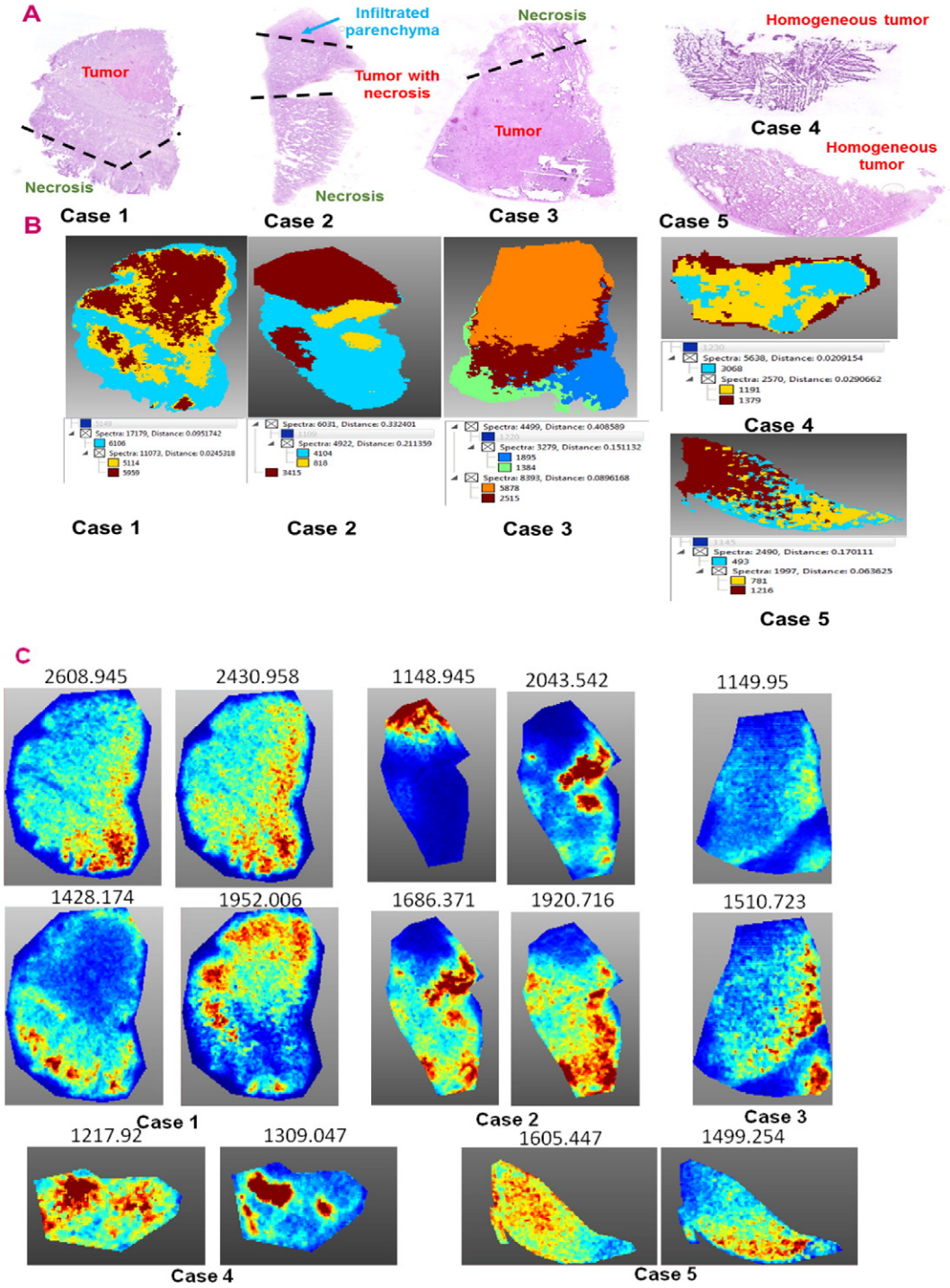

Fig. 2. Histological and MALDI MSI data of the 5 grade III glioma cases. (A) Scanned pictures after hematoxylin-eosin staining and anathomo-pathologist annotations. (B) Individual segmentation maps for each case. The segmentation map shows 3 clusters for cases number 1, 2, 4 and 5 and 4 clusters for case number 3. Colors represent molecularly different regions as shown in the corresponding dendrogram. Note that for 2 different tissues, similar colors are not equivalent to similar molecular groups. Dark blue clusters are masked on segmentation because those correspond to the off-tissue spectra. (C) MALDI MSI images of characteristics *m/z* observed for the different cases. (D) Global segmentation maps of all tissues together. Colors represent molecularly different regions as shown in the corresponding dendrogram. The segmentation map gives 4 main clusters. Cases number 1 and 4 are molecularly similar and are represented in blue (Group 1). Cases number 2, 3 and 5 are grouped together based on their molecular profiles and are represented in orange, green and brown. These last cases can be divided into two groups with the brown region (Group 2) in one group and green/orange regions in another group (Group 3). Microextraction spots (1.1, 1.2, 1.3 for case 1, 5.1, 5.2, 5.3 for case 2, 6.1, 6.2 for case 4, 20.1, 20.2, 20.3 for case 3, 22.1, 22.2 and 22.3 for case 5) are localized on the segmentation maps in the different ROIs of each tissue and are indicated by a white cross.

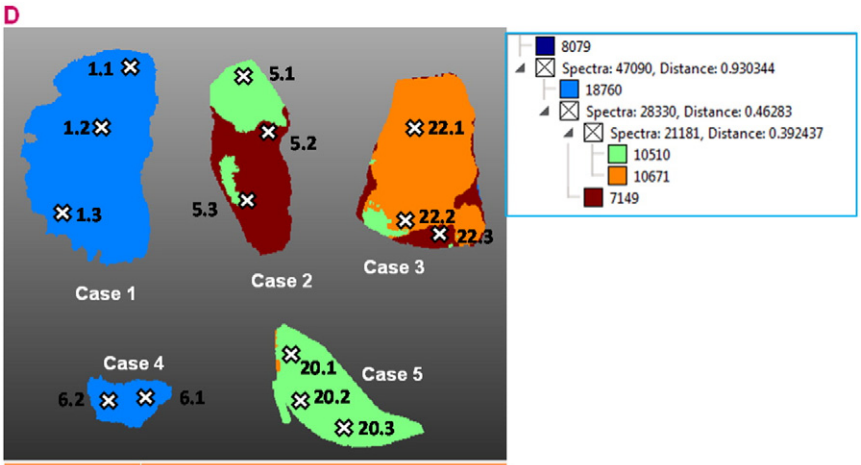

Segments	Microextraction points
Blue	1.1/1.2/1.3/6.1/6.2
Brown	5.2/5.3/22.3
Green + Orange	20.1/20.2/20.3/5.1/22.1/22.2

Fig. 2 (*continued*).

number 1 and 4 (corresponding to the blue region) from the other ones (Fig. 3A). Cases number 2, 3 and 5 were molecularly closer as they belonged to the same branch of the dendrogram of the samples. This branch is then divided into samples 5.2, 5.3 and 22.3 (corresponding to the brown region) for one part and samples 20.1, 20.2, 20.3, 5.1, 22.1 and 22.2 (corresponding to the green/orange region) for the other part (Fig. 3A) which can be associated to green/orange regions. This classification based on the proteins' up or downregulation expression profiles, is well in line with the classification obtained by the clustering of the MALDI MSI data (Fig. 2D). Indeed, MALDI MSI classified cases number 1 and 4 together and cases number 2, 3 and 5 together. These three last samples are molecularly heterogeneous because different regions are found within each tissue separating points 5.2, 5.3 and 22.3 and 5.1, 20.1, 20.2, 20.3, 22.1 and 22.2 (Fig. 2D). We decided to classify samples 5.1, 20.1, 20.2, 20.3, 22.1 and 22.2 together because they belong to the same branch of the tree. They are molecularly closed based on the spatial segmentation.

Thus, to simplify the denomination of each group, we named them Group 1, Group 2 and Group 3 in the samples' dendrogram. Extraction spots 1.1, 1.2, 1.3, 6.1 and 6.2 belong to Group 1. Group 2 corresponded to extraction points 5.2, 5.3 and 22.3. Group 3 is constituted by extraction spots 20.1, 20.2, 20.3, 5.1, 22.1 and 22.2 (Fig. 3A). Considering the overexpressed proteins showed in red in the heatmap, 386 proteins extracted from the protein dendrogram are overexpressed in Group 1, 198 in Group 2 and 315 in Group 3. The overexpressed proteins specific to each of these 3 clusters are listed in Suppl. Table 2. Comparison of the biological process and molecular functions of the three groups showed that Group 1 was in the majority involved in metabolic processes, binding and catalytic activity (Fig. 3B) and included specific proteins such as chaperones and nucleic acid binding proteins (Fig. 3C). STRING network analysis reveals two major clusters *i.e.* RNA splicing and proteins localized in endoplasmic reticulum, and the RNA catabolic process (Fig. 3D). Several proteins are of particular interest due to their involvement in glioma and tumor cell growth promotion *e.g.* BAG family molecular chaperone regulator 3 (BAG3), Hematopoietic lineage cell-specific protein (HS1), Leukotriene A-4 hydrolase (LTA4H), Programmed cell death 6-interacting protein (PDC6IP), Pre-B-cell leukemia transcription factor-interacting protein 1 (PBXIP1). Group 2 is found to be specifically involved in reproductive biological functions but also in developmental, cellular and metabolic processes (Fig. 3B). For protein class, proteins in group 2 are more involved in the cytoskeleton and hydrolase (Fig. 3C). No specific cluster can be observed with STRING analysis for this group (Supp. Fig. 1). Interestingly, some of the proteins identified have never been described in Glioma such as Lethal (2) giant larvae protein homolog 1 (LLGL1), MTSS1-like protein (MTSS1L), Shootin-1 (KIAA1598), and LanC-like protein 1 (LANC1). By contrast, Isocitrate dehydrogenase [NADP] cytoplasmic (IDH1 and IDH2), Breast carcinoma-amplified sequence 1 (BCAS1), Optineurin (OPTN), and WD repeat-containing protein 44 (WDR44) are overexpressed in group 2 and are proteins known to play a key role in aggressive glioma (Supp. Data 2). For group 3, binding, receptor activity, and metabolic activity, are the most important modulated functions (Fig. 3B). STRING analysis shows the presence of two clusters one being related to the metabolic process and the other one to endocytosis (Supp. Fig. 2). IDH3, IDH3A, IDH3G, Neural cell adhesion molecule L1-like protein (CHL1), Disks large homolog (DLG1 and DLG2), Neuronal growth regulator 1 (NGR1), Rho-associated protein kinase 2 (ROCK2), Neural cell adhesion molecule L1 (L1CAM), and Tumor protein D52 (TDP52) are overexpressed in group 3 and are known to be involved in glioma.

Analysis of molecular pathways was then performed on the overexpressed proteins extracted from the heatmap of Fig. 2A for each sample group (Fig. 4). Differential distribution of unique & common/intersected biological and functional pathways among the three different groups (Groups 1, 2 and 3) are depicted in Fig. 4A,B,C. Unique statistically significant pathways were identified including 61 pathways for group 3; 43 pathways for group 2; and 58 pathways for group 1 (please refer to Suppl. Tables 6, 7, and 8 for the identity of each of the unique pathways). Combined differential pathways were analyzed across the three groups. 17 pathways were shared between groups 2 & 3, 20 pathways were shared between groups 2 & 1, and 2 pathways were shared between groups 1 & 3. 20 pathways were shared among the groups 1, 2 & 3. Please refer to Suppl. Tables 9 & 10 for the pathways' identity, implicated proteins and the specific *P* value of each of the unique pathways. Integrated Venn diagram analysis was performed using "the InteractiVenn": a web-based tool for the analysis of complex data sets [48]. See Supp. Tables 3, 4 and 5 as supplementary data for the listed differential pathways. Overexpressed proteins in group 1 (Fig. 4A) are involved in neoplasia, innate immune response, autophagy, response to oxidative stress, mRNA metabolism, protein folding, spliceosome, and regulation of translation which is line with neoplasia and necrosis. For

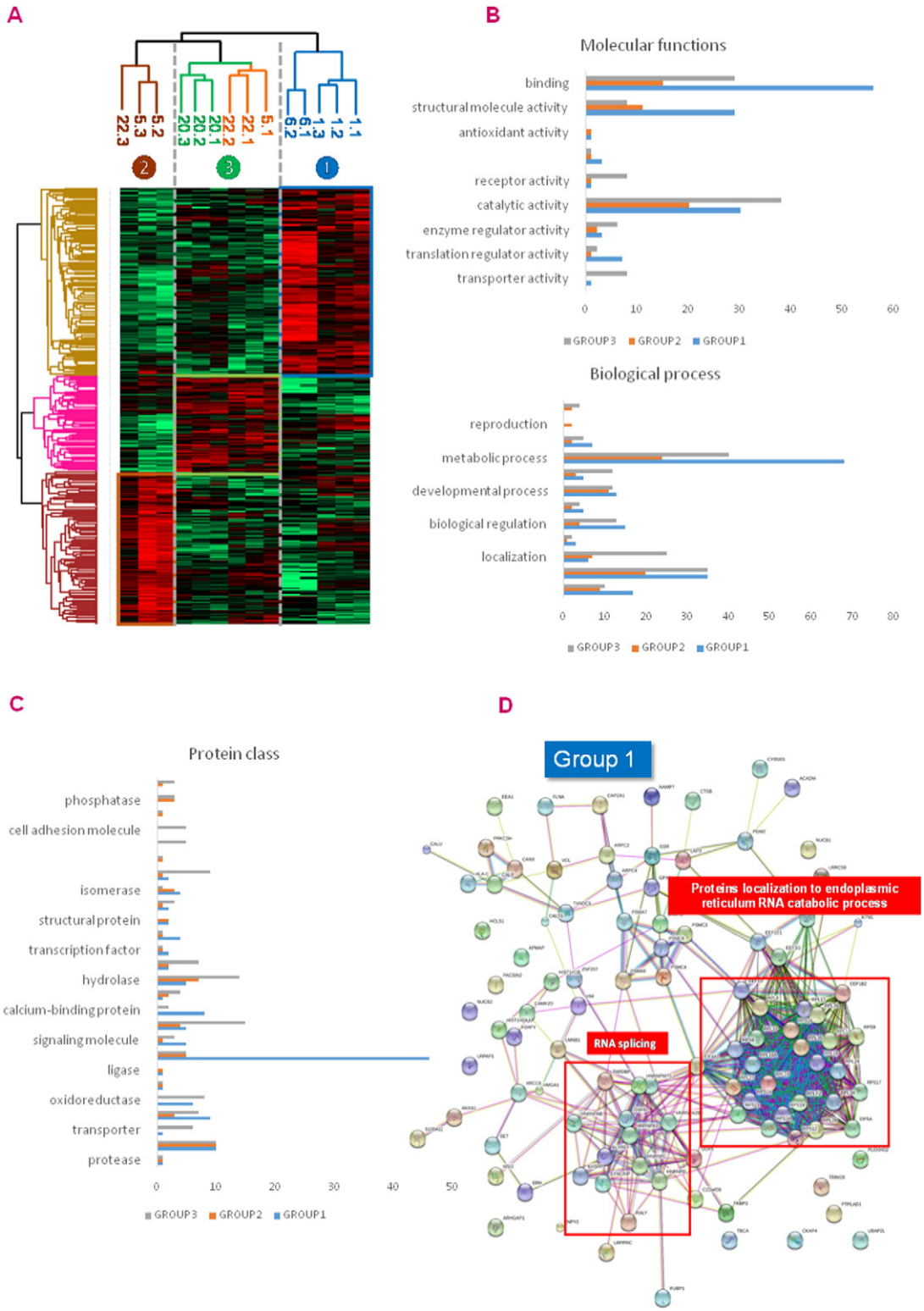

Fig. 3. Shotgun microproteomics analysis. Shotgun proteomics was performed after on-tissue trypsin digestion followed by microextraction at the spots determined from MALDI MSI data. (A) Heat map of proteins with different regulation profiles as determined after label free quantification in the three groups highlighting the presence of 3 clusters. (B) Diagrams giving the molecular functions and biological processes associated to the overregulated proteins after analyzing protein clusters with Panther software. (C) Protein classes of the overregulated proteins after analyzing protein clusters with Panther software. (D) STRING analysis of proteins overregulated in group 1.

group 2 (Fig. 4B), the subnetwork is mainly glioma, inflammation, microglia activation, neoplasma and metastasis, cell migration, motility, and microtubule cytoskeleton assembly which is line with aggressive glioma. For group 3 (Fig. 4C), the pattern is more related to nerve cell differentiation, neurite outgrowth, axon guidance, filopodia formation, and secretory pathway which is line with neuronal stem cell profile.

We, therefore, characterized each group thanks to its protein expression profiles. Group 1 is mainly associated with neoplasia showing

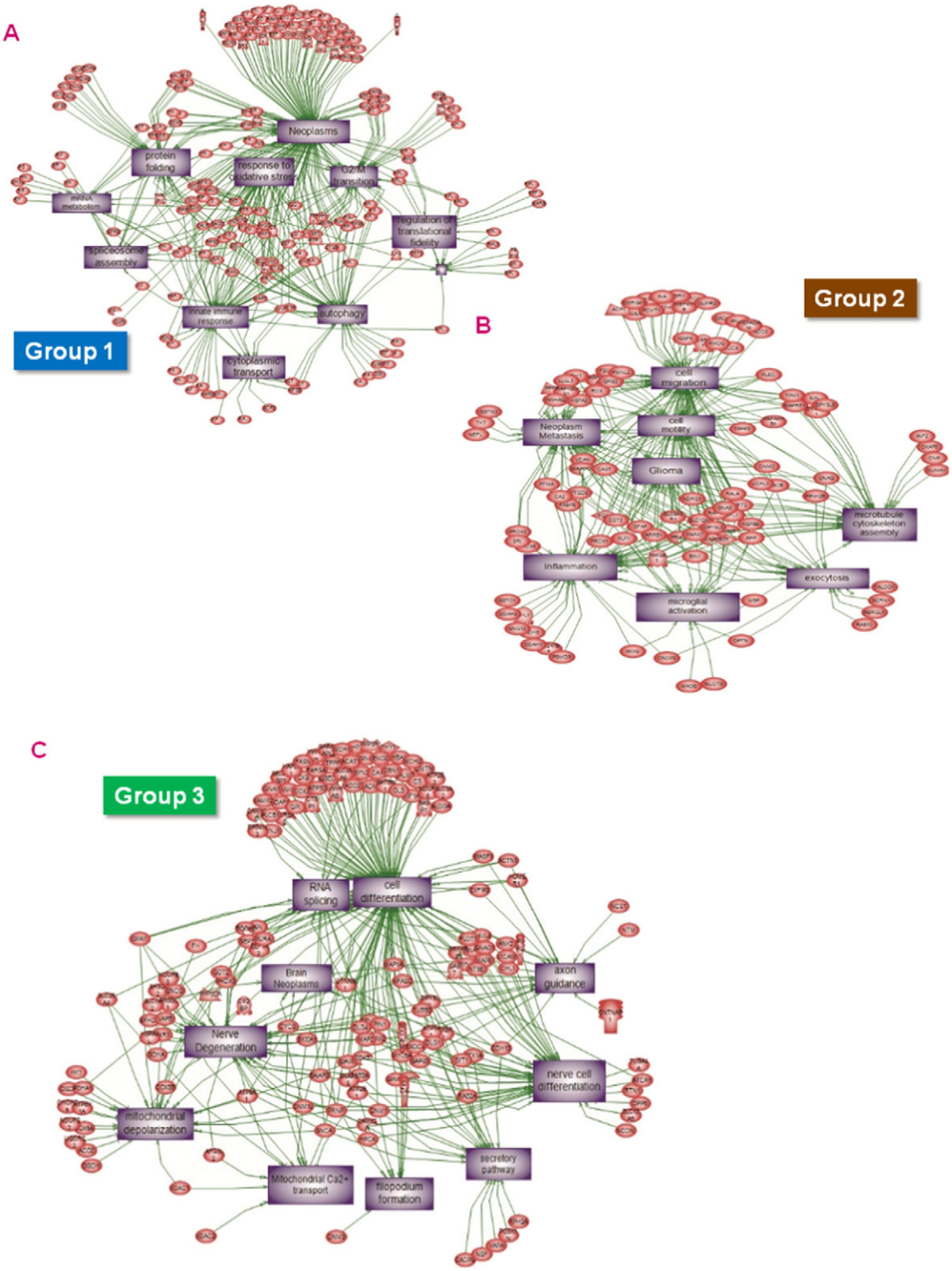

Fig. 4. Molecular pathways associated to overregulated proteins. Overregulated proteins in (A) Group 1, (B) Group 2 and (C) Group 3.

many proteins involved in tumor cell growth. Group 1 corresponds to aggressive tumor. Group 2 regroups many proteins involved in inflammation and metastasis. Group 3 has a neuronal stem cell profile with proteins specific to nerve cell differentiation and neurite outgrowth.

3.4. Validation test and association to clinical data

A classification model was built using the predefined groups obtained by the global spatial segmentation (Fig. 2D). For each group, 5 data subsets (training group) were selected for the classification (Fig. 5A, top). This classification model was tested on another subset of the same groups (blind test group) and then applied to a blind set of 5 new samples originating from 5 new patients (case 6 to case 10) (Fig. 5A, bottom). As a result, cases number 6 (a part), 8 and 10 (a part) are classified within group 1 as confirmed by the distribution of ions at m/z 1599.218 and 2281.756, which are found in cases 1, 4, 8 and partially in 6 and in 10 (Fig. 5B). Case number 9 is very similar to the large brown area of case number 2 and therefore belongs

to group 2. Ions at *m/z* 1155.958 and 1433.345 support the similarity of cases number 2 and 9 (Fig. 5B). Group 3 regroups cases number 5, 7 with a part of cases number 2, 3, 6 and 9. Ions at *m/z* 1149.785 and 1540.143 were specific of this group (Fig. 5B). From these data, we can conclude that group 1 regroups cases number 1, 4, 8, part of 6 and part of 10. Groups 2 and 3 were difficult to separate completely due to the fact that some parts of the tissues belong to one group and the other to another group. However, we previously observed on the heat map and on the global segmentation that these two groups were molecularly very close (Fig. 2D and 3A). Thus, taking into account this point, the two groups can be merged as a single group that will be named as "group 2" which is divided into two sub-groups. Thus, cases 2, 3, 5, 7, part of 6 and part of 9 belonged to group 2.

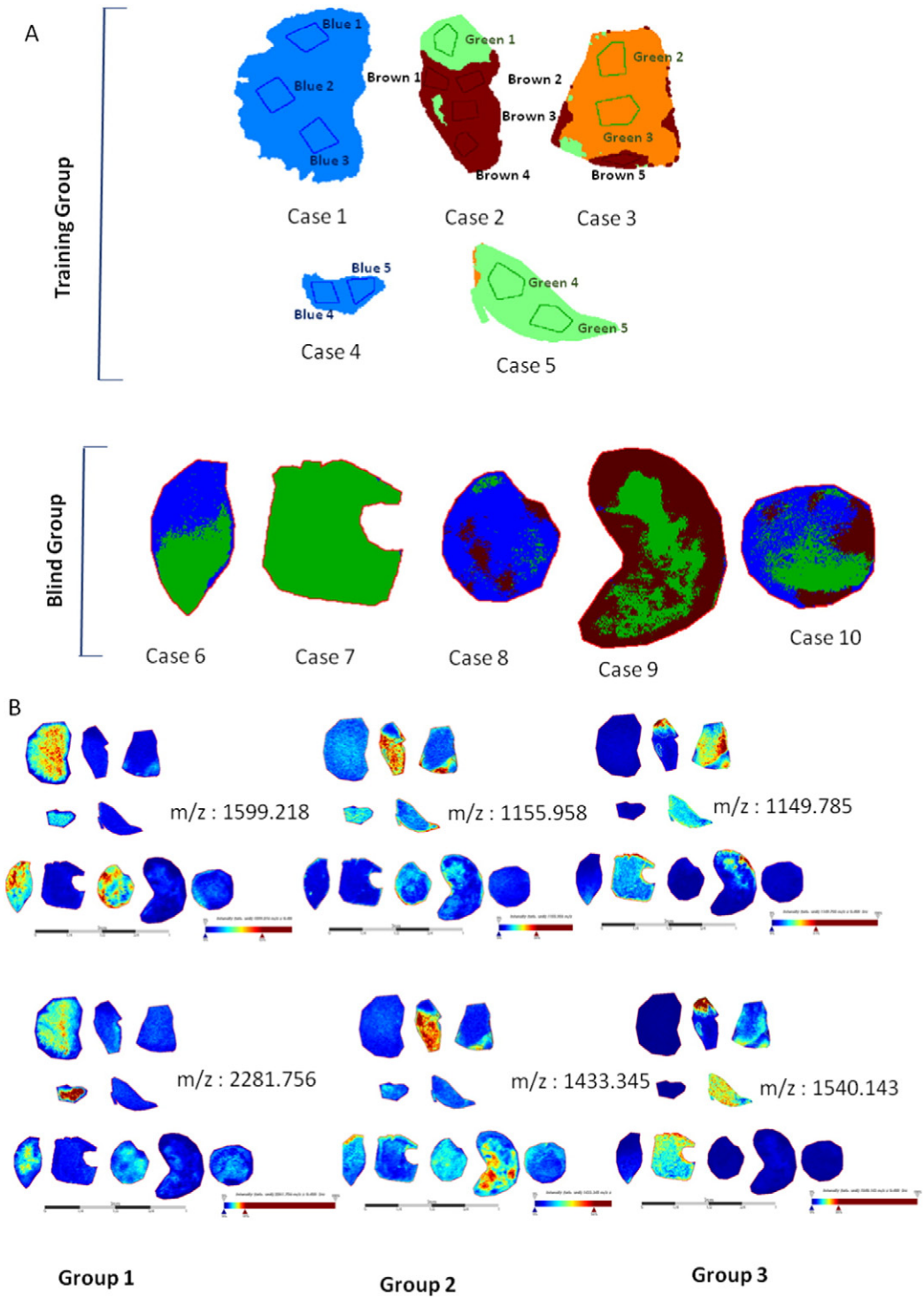

Fig. 5. Test of the classification on 5 additional patients. (A) A classification model was generated. The training group presents three classes (blue; green/orange and brown). For each class, 3 subset regions were used for training and 2 subset regions for validation. The built model was then used to classify five new samples. Sample 7 is classified in the green region. Sample 8 is classified in the blue region and samples 6, 9 and 10 are heterogeneous. (B) Specific *m/z* images were extracted for each group. (C) MALDI imaging segmentation map of the 10 tissues. The segmentation map shows 2 main clusters: blue vs orange/brown. Colors represent molecularly different regions.

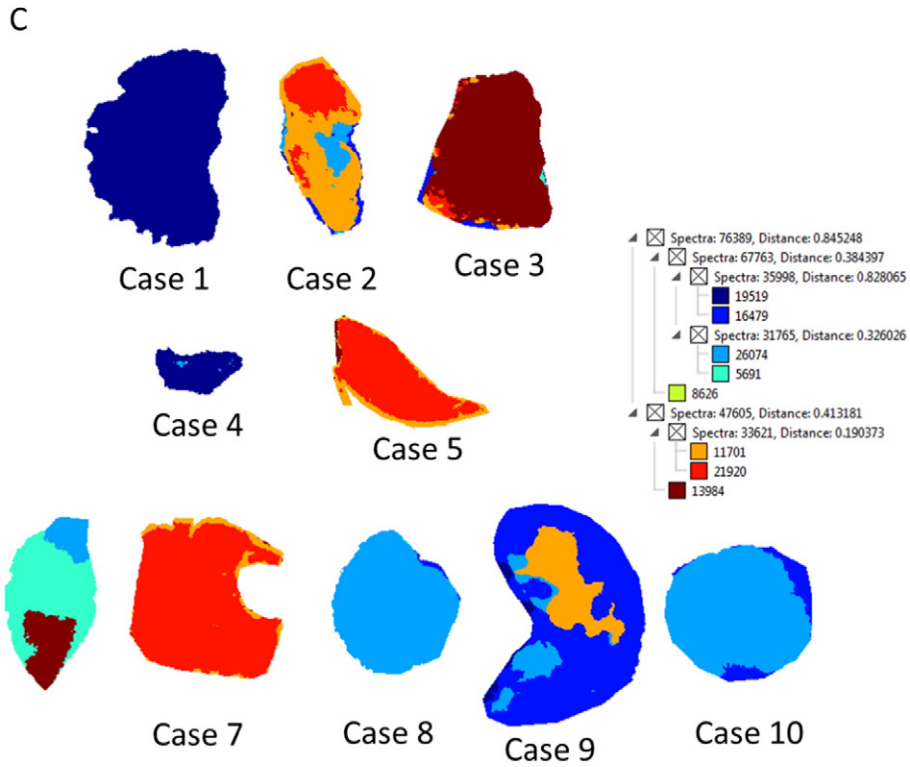

Fig. 5 (*continued*).

Then, a complete unsupervised segmentation using the 10 samples was realized (Fig. 5C). From this segmentation, only two main groups can be deduced. The first regroups cases number 1, 4, 8 and 10 (deep and light blue). The second one regroups cases number 2, 3, 5 and 7 (red, orange and brown). Cases number 6 and 9 are more difficult to classify, the tissues presenting molecular signatures characteristic of both groups.

Taking into account these two groups, we searched which proteins were only expressed in each of these groups to find potential biomarkers (Table 2). Sixteen proteins have been detected in group 1 *i.e.* HLA-DRA, Destrin (DSTN), CD74, Glucosidase alpha acid (GAA), P450 oxydoreductase (POR), Ribosomal Protein L12 (RPL12), Scaffold attachment factor B2 (SAFB2), Poly(A) binding protein nuclear 1 (PABPN1), CDC5 cell division cycle 5-like (CDC5L), Golgi reassembly stacking protein 2 (GORASP2), Golgi integral membrane protein 4 (GOLIM4), Ribophorin II (RPN2), Nidogen 1 (NID1), chromobox homolog 5 (CBX5), Aspartate beta-hydrolase (ASPH) (Table 2). Group 2 contains Myelin basic protein (MBP), CYBRD1, Small VCP:p97 interacting protein (SVIP), Ermin (ERMN), Anillin (ANLN), Oligodendrocytic myelin paranormal and inner loop protein (OPALIN), Glycolipid transfer protein (GLTP), Hyaluronan and proteoglycan link protein 2 (HAPLN2), MAP6 domain containing 1 (MAP6D1), CD9, Glycerol-3 phosphatase dehydrogenase-1 (GPD1), Ectonucleotide Pyrophosphatase/Phosphodiesterase 6 (ENPP6), Myosin (MYO1D), and Dynein cytoplasmic 1 intermediate chain 1 (DYNC1I1) (Table 2).

Even though the patient cohort remains limited, if we compare the grouping obtained using MS-based molecular data, we do not observe a correlation with the pathologist classification as performed using the WH0 2007 classification [1]. If we also look for comparison with the molecular markers such as IDH1 mutation and 1p19q codeletion or the methylation status of MGMT which are some of the main features of the newly released WHO 2016 classification [3], no direct correlation is observed (although this is difficult because there is only 1 IDH1 negative case in the patient's cohort) (see Table 1). Indeed, Group 1 regroups cases 1, 4, 8, and 10. Out of these 4 cases, it can be retrieved from the clinical data that 4 have ATRX loss, 3 are EGRF positive, 4 are P53 positive, 3 are IDH1 positive and 4 have no 1p/19q codeletion. All are MGMT 5 methylated. 3 of the 5 have abnormalities on chromosomes 7 and 10, *i.e.* 2 are 7p gain and 10p gain, one 7 loss and 1 no abnormalities. For Group 2, including cases 2, 3, 5 and 7, 3 have ATRX expressed, 3 P53 negative, 2 have 1p/19q codeletion and 2 none. All are MGMT methylated and IDH1 positive. For chromosome 7 and 10, 3 have no abnormalities. Cases 6 and 9 present a mixed up of the two other groups. Case 6 is negative in IDH R132H immunocytochemistry, but the molecular analysis confirms the presence of IDH1 mutation. It is ATRX loss, P53 negative, no codeletion 1p/19q and is EGRF positive. It has no MGMT methylation and has chromosome 7 loss. Case 9 is IDH1 positive. It presents a 1p/19q codeletion. It express ATRX, MGMT methylation and no chromosome 7 and 10 abnormalities. It must be noticed that the molecular data are only reported for defined targets when our approach is performed on large scale data. Moreover, the proteomics data are collected in different parts of the tissue for tissues showing a heterogeneous profile when the biological data are only confirmed as present or absent for a tissue. It is also important to notice that no correlation is found between the MSI/Proteomics classification and the histological one.

4. Discussion

Previous proteomics studies have been reported on Glioma. These include a large panel of different studies based of different methodologies and including profiles determined from glioma cell lines [49–51], animal models [49–52], patients fluids [50,51,53] and patients samples [50,51,53–59]. To date, mainly two methodologies were used for such glioma proteomics studies namely gel-based protein profiling [56,57,59] and quantitative proteomics [55,60–63]. However, none of these previous studies used MALDI MSI methodology coupled to label-free tissue microproteomics [33,34,64]. The MALDI MSI methodology authorizes molecular imaging of different classes of biomolecules obtained from tissue samples without requiring antibodies, tagged or

Table 2
Proteins specifically identified by Shotgun microproteomics in group 1 and group 2. Proteins are groups according to the microextraction spot in which they are found.

Identified proteins	Protein names	Gene names
Group 1		
Common to 1.1/1.2/1.3/6.1/6.2		
Q30118	HLA class II histocompatibility antigen, DR alpha chain	HLA-DRA
F6RFD5	Destrin	DSTN
P04233-2	HLA class II histocompatibility antigen gamma chain	CD74
P10253	Lysosomal alpha-glucosidase;76 kDa lysosomal alpha-glucosidase;70 kDa lysosomal alpha-glucosidase	GAA
Common to 1.1/1.2/6.1/6.2		
H0Y4R2	NADPH--cytochrome P450 reductase	POR
P30050	60S ribosomal protein L12	RPL12
Q14151	Scaffold attachment factor B2	SAFB2
Q86U42-2	Polyadenylate-binding protein 2	PABPN1
Q99459	Cell division cycle 5-like protein	CDC5L
Q9H8Y8-2	Golgi reassembly-stacking protein 2	GORASP2
Common to 1.1/1.3/6.1/6.2		
F8W785	Golgi integral membrane protein 4	GOLIM4
P04844-2	Dolichyl-diphosphooligosaccharide-protein glycosyltransferase subunit 2	RPN2
P14543-2	Nidogen-1	NID1
P45973	Chromobox protein homolog 5	CBX5
Q12797-10	Aspartyl/asparaginyl beta-hydroxylase	ASPH
F8W785	Golgi integral membrane protein 4	GOLIM4
Group 2		
Common to 20.1/20.2/20.3/22.1/22.2/22.3/5.1/5.2/5.3		
P02686-4	Myelin basic protein	MBP
Q53TN4-3	Cytochrome b reductase 1	CYBRD1
Q8NHG7	Small VCP/p97-interacting protein	SVIP
Q8TAM6	Ermin	ERMN
Q9NQW6	Actin-binding protein anillin	ANLN
Common to 20.1/20.3/22.1/22.2/22.3/5.1/5.2/5.3		
A0A0A0MTN4	Opalin	OPALIN
F5H0U5	Glycolipid transfer protein	GLTP
Q9GZV7	Hyaluronan and proteoglycan link protein 2	HAPLN2
Q9H9H5	MAP6 domain-containing protein 1	MAP6D1
Common to 20.1/20.2/20.3/22.1/22.2/22.3/5.1/5.2		
A6NNI4	Tetraspanin; CD9 antigen	CD9
P21695-2	Glycerol-3-phosphate dehydrogenase [NAD(+)], cytoplasmic	GPD1
Q6UWR7	Ectonucleotide pyrophosphatase/phosphodiesterase family member 6	ENPP6
Common to 20.1/20.2/20.3/22.1/22.2/5.1/5.2/5.3		
K7EIG7	Unconventional myosin-Id	MYO1D
Common to 20.2/20.3/22.1/22.2/22.3/5.1/5.2/5.3		
O14576-4	Cytoplasmic dynein 1 intermediate chain 1	DYNC1I1

labeled probes [31]. Here we were interested in evaluating the classification resulting from the non-supervised analysis using MALDI MSI data of tryptic peptides issuing from protein digestion and compare this to the pathologist annotation and the patients molecular data. Microproteomics was combined to the non-supervised clustering to evaluate the observation of specific signaling pathways and retrieve corresponding biomarkers. A set of five grade III glioma samples were thus analyzed by MALDI MSI looking to the digestion peptides of proteins followed by individual and global non-supervised hierarchical clustering. In our study, molecular discrepancies were identified between annotations of the neuropathologist and the molecular histology done by MALDI MSI, with more regions of interest identified by the MALDI MSI analysis. Indeed, based on the WHO classification, some samples are categorized as homogeneous tumors whereas MALDI MSI data clearly state that the tumor is molecularly heterogeneous. This point tends to demonstrate the fact that MALDI MSI can be a tool for helping pathologists to improve their diagnoses by obtaining additional information. The global clustering of the five samples revealed three groups of different molecular profiles. Proteins up-and down-regulated or specific to these groups were further identified by Shotgun tissue microproteomics. Majority of the proteins identified in group 1 are involved in the metabolic process, binding and catalytic activity. This was confirmed by signaling pathways and interactions found using functional analysis tools. All pathways are involved in neoplasia, innate immune response, autophagy, response to oxidative stress, mRNA metabolism, protein folding, spliceosome, and regulation of translation. Part of the proteins identified within this group were also found in the study of Polisetty et al. where differentially expressed proteins in anaplastic astrocytoma were mainly associated with mRNA processing [54]. Group 2 is specifically involved in reproductive biological functions but also in developmental, cellular and metabolic processes. The pathway analysis confirms that this group is mainly involved in glioma pathology, inflammation, microglia activation, neoplasm and metastasis, cell migration, motility and microtubule cytoskeleton assembly. Microglia/macrophages infiltration has previously been reported in glioma and these cells are responsible for the chemoresistance, metastasis and tumor progression [65–67]. Group 3 is more related to nerve cell differentiation, neurite outgrowth, axon guidance, filopodia formation and the secretory pathway.

Then, the test of the classification was realized by using 5 blind samples with MALDI MSI. They were classified into two main groups *i.e.* group 1 and a merge of group 2 and group 3. This classification is supported by the segmentation performed on the 10 samples. Despite that only a few samples were evaluated in this study, some common molecular features were shared between samples among the proteomics subgroups. Group 1 is constituted by specific proteins involved in major histocompatibility complex, mRNA formation, DNA and histone H3 binding, cell trafficking in Golgi apparatus, metabolism, cell cycle and cell attachment. CD74 and HLA-DR are linked to macrophages or microglia tumor infiltration [68]. Expression of CD74 in high-grade glioma is associated with resistance to temozolomide treatment [69]. GORASP2, GOLIM4, CD74, and HLA-DR have recently been identified in glioblastoma membrane proteomic study [63]. RNP2, as well as CBX5, are considered as markers of glioma and seem to be therapeutic targets [70,71]. Considering SAFB2, PABPN1, and CDC5L, these proteins are involved in RNA splicing and recently in non-coding RNA turnover [72–74]. Group 2 contains proteins known to be implicated in glioma-like Ermin, HAPLN2, MAP6D1, ENPP6, DYNC1I1, and MBP [75]. Moreover, Anillin, OPALIN and GPD1 are markers of glioma stem cells [76].

In conclusion, we demonstrated that the use of MALDI MSI combined to microproteomics might allow the generation of tumor classification associated with the identification of specific signaling pathways and a set of potential markers. In this first study on 10 grade III glioma patients, we show that the classification allows for two main groups to be distinguished. First data demonstrate that a direct comparison to the molecular and clinical data is not straightforward. MALDI MSI/proteomics data do not seem to show correlation with the histological type which is in line with the recently rebuilt classification based on the molecular data. MALDI MSI demonstrates a clear advantage to highlight spatial molecular heterogeneity of glioma which is associated to different molecular pathways and seems to relate to different subgroups of patients. Correlation with molecular data is not immediate and would necessitate a larger patient cohort to be investigated. This will also require the development of bioinformatics tools that can cope with the integration of clinical, histological, and targeted molecular data to our large scale non-targeted proteomics data.

This study is prospective, and this approach needs to be realized on a larger cohort of patients where we will be able to correlate proteomics data to genomic data. However, some interesting points can still be drawn. In fact group 1 integrates several proteins linked to RNA splicing, mRNA expression and regulation of specific transcripts but also on the turnover of long noncoding RNAs (lncRNAs). This can be associated with the presence of several alternative proteins issued from alternative ORF [42]. We detect using our *in silico* AltORF

Table 3
Human alternative proteins identified by Shotgun microproteomics that don't show any correspondence to reference human proteins found in the conventional databases.

Gene references	Whole ID proteomics	Group 1	Group 2
altHES2	IP_058211.1		
altSFPQ	IP_062363.1	IP_062363.1	
altEDARADD	IP_079312.1	IP_079312.1	
altRYR2	IP_079402.1		IP_079402.1
altLMAN2L	IP_088021.1		IP_088021.1
altPLA2R1	IP_091451.1	IP_091451.1	
altTTN	IP_092840.1	IP_092840.1	
altSTC2	IP_134213.1		
altSNHG18	IP_135449.1		IP_135449.1
altFOXF2	IP_136674.1		
altPRDM13	IP_143952.1		
altHCG18	IP_148329.1		IP_148329.1
altRP3-323P13.2	IP_149055.1		IP_149055.1
altPON2	IP_154527.1		IP_154527.1
altLINC00094	IP_180218.1		IP_180218.1
altANXA8	IP_183058.1	IP_183058.1	
altZCCHC24	IP_185288.1	IP_185288.1	
altAC068858.1	IP_204724.1	IP_204724.1	
altTRAF7	IP_240015.1		IP_240015.1
altHIF3A	IP_276654.1	IP_276654.1	
altIGSF5	IP_289664.1	IP_289664.1	
altCSF2RB	IP_294011.1	IP_294011.1	

databank, 22 alternative proteins in the whole of the proteomics data without correspondence with known human proteins and the specific AltProt of each group was also detected (Table 3). Such alternative proteins can be useful for diagnosis and prognosis and need to be investigated in this way.

By identifying protein expression, proteomics analysis may add new information to improve the classification of gliomas and to identify novel potential therapeutic targets. This kind of analysis can provide new candidate biomarkers and can improve the knowledge of glioma biology. Our results need further validation on a larger prospective cohort of gliomas with various IDH and 1p19q codeletion statuses.

Supplementary data to this article can be found online at http://dx.doi.org/10.1016/j.bbapap.2016.11.012.

Conflict of interest

We declare that the authors have no conflict of interest.

Competing financial interests

The authors declare no competing financial interests.

Contributions

ELR: conception and design, data acquisition, data analysis, manuscript writing, final approval.

MD: conception and design, data acquisition, data analysis, manuscript writing, final approval.

MW: conception and design, data acquisition, data analysis, manuscript writing, final approval.

FZ: data acquisition, manuscript writing, final approval.

FE: conception and design, data acquisition, manuscript writing, final approval.

CAM: conception and design, data acquisition, data analysis, manuscript writing, final approval.

NR: conception and design, data acquisition, data analysis, manuscript writing, final approval.

FK: data analysis, manuscript writing, final approval.

MS: conception and design, data acquisition, data analysis, manuscript writing, final approval.

IF: conception and design, data acquisition, data analysis, manuscript writing, final approval.

Transparency document

The Transparency document associated with this article can be found, in the online version.

Acknowledgements

This research was supported by grants from the Ministère de L'Education Nationale, de L'Enseignement Supérieur et de la Recherche, ANR (IF), the Université de Lille (MD), Métropole Européenne de Lille (MD), SIRIC ONCOLille (IF, MD) Grant INCa-DGOS-Inserm 6041aa, and INSERM. We would like to thank Sylvie Janas and the Tumorothèque Régionale of Nord Pas de Calais and Clic-Imaging Platform of Université de Lille. We also would like to thank Prof. Xavier Roucou (Université deSherbrooke, Canada) for supplying the library of alternative proteins.

References

[1] D.N. Louis, H. Ohgaki, O.D. Wiestler, W.K. Cavenee, P.C. Burger, A. Jouvet, B.W. Scheithauer, P. Kleihues, The 2007 WHO classification of tumours of the central nervous system, Acta Neuropathol. 114 (2007) 97–109.
[2] M.J. van den Bent, Interobserver variation of the histopathological diagnosis in clinical trials on glioma: a clinician's perspective, Acta Neuropathol. 120 (2010) 297–304.
[3] M. Weller, R.G. Weber, E. Willscher, V. Riehmer, B. Hentschel, M. Kreuz, J. Felsberg, U. Beyer, H. Loffler-Wirth, K. Kaulich, J.P. Steinbach, C. Hartmann, D. Gramatzki, J. Schramm, M. Westphal, G. Schackert, M. Simon, T. Martens, J. Bostrom, C. Hagel, M. Sabel, D. Krex, J.C. Tonn, W. Wick, S. Noell, U. Schlegel, B. Radlwimmer, T. Pietsch, M. Loeffler, A. von Deimling, H. Binder, G. Reifenberger, Molecular classification of diffuse cerebral WHO grade II/III gliomas using genome- and transcriptome-wide profiling improves stratification of prognostically distinct patient groups, Acta Neuropathol 129 (2015) 679–693.
[4] W. Wick, M. Weller, Anaplastic glioma. Neuropathology, molecular diagnostics and current study concepts, Nervenarzt 81 (2010) 928–930 (932-925).
[5] N. Hata, S.O. Suzuki, H. Murata, R. Hatae, Y. Akagi, Y. Sangatsuda, T. Amano, K. Yoshimoto, T. Tahira, M. Mizoguchi, Genetic analysis of a case of glioblastoma with oligodendroglial component arising during the progression of diffuse astrocytoma, Pathol Oncol Res 21 (2015) 839–843.
[6] K. Fukuoka, T. Yanagisawa, Y. Watanabe, T. Suzuki, M. Shirahata, J. Adachi, K. Mishima, T. Fujimaki, M. Matsutani, S. Wada, A. Sasaki, R. Nishikawa, Brainstem oligodendroglial tumors in children: two case reports and review of literatures, Childs Nerv. Syst. 31 (2015) 449–455.
[7] L.A. Cooper, D.A. Gutman, Q. Long, B.A. Johnson, S.R. Cholleti, T. Kurc, J.H. Saltz, D.J. Brat, C.S. Moreno, The proneural molecular signature is enriched in oligodendrogliomas and predicts improved survival among diffuse gliomas, PLoS One 5 (2010), e12548.
[8] A. Idbaih, A. Omuro, F. Ducray, K. Hoang-Xuan, Molecular genetic markers as predictors of response to chemotherapy in gliomas, Curr. Opin. Oncol. 19 (2007) 606–611.
[9] P.J. Killela, C.J. Pirozzi, Z.J. Reitman, S. Jones, B.A. Rasheed, E. Lipp, H. Friedman, A.H. Friedman, Y. He, R.E. McLendon, The genetic landscape of anaplastic astrocytoma, Oncotarget 5 (2014) 1452–1457.
[10] P.J. Killela, C.J. Pirozzi, P. Healy, Z.J. Reitman, E. Lipp, B.A. Rasheed, R. Yang, B.H. Diplas, Z. Wang, P.K. Greer, Mutations in IDH1, IDH2, and in the TERT promoter define clinically distinct subgroups of adult malignant gliomas, Oncotarget 5 (2014) 1515–1525.
[11] Y. Jiao, P.J. Killela, Z.J. Reitman, B.A. Rasheed, C.M. Heaphy, R.F. de Wilde, F.J. Rodriguez, S. Rosemberg, S.M. Obashinjo, S.K.N. Marie, Frequent ATRX, CIC, FUBP1 and IDH1 mutations refine the classification of malignant gliomas, Oncotarget 3 (2012) 709–722.
[12] B. Wiestler, D. Capper, T. Holland-Letz, A. Korshunov, A. von Deimling, S.M. Pfister, M. Platten, M. Weller, W. Wick, ATRX loss refines the classification of anaplastic gliomas and identifies a subgroup of IDH mutant astrocytic tumors with better prognosis, Acta Neuropathol. 126 (2013) 443–451.
[13] G. Cairncross, M. Wang, E. Shaw, R. Jenkins, D. Brachman, J. Buckner, K. Fink, L. Souhami, N. Laperriere, W. Curran, Phase III trial of chemoradiotherapy for anaplastic oligodendroglioma: long-term results of RTOG 9402, J. Clin. Oncol. 31 (2013) 337–343.
[14] G. Cairncross, B. Berkey, E. Shaw, R. Jenkins, B. Scheithauer, D. Brachman, J. Buckner, K. Fink, L. Souhami, N. Laperierre, Phase III trial of chemotherapy plus radiotherapy compared with radiotherapy alone for pure and mixed anaplastic oligodendroglioma: Intergroup Radiation Therapy Oncology Group Trial 9402, J. Clin. Oncol. 24 (2006) 2707–2714.
[15] M. Weiler, W. Wick, Molecular predictors of outcome in low-grade glioma, Curr. Opin. Neurol. 25 (2012) 767–773.
[16] X.-Y. Liu, N. Gerges, A. Korshunov, N. Sabha, D.-A. Khuong-Quang, A.M. Fontebasso, A. Fleming, D. Hadjadj, J. Schwartzentruber, J. Majewski, Frequent ATRX mutations and loss of expression in adult diffuse astrocytic tumors carrying IDH1/IDH2 and TP53 mutations, Acta Neuropathol. 124 (2012) 615–625.
[17] D.E. Reuss, F. Sahm, D. Schrimpf, B. Wiestler, D. Capper, C. Koelsche, L. Schweizer, A. Korshunov, D.T. Jones, V. Hovestadt, ATRX and IDH1-R132H immunohistochemistry with subsequent copy number analysis and IDH sequencing as a basis for an

"integrated" diagnostic approach for adult astrocytoma, oligodendroglioma and glioblastoma, Acta Neuropathol. 129 (2015) 133–146.
[18] J.E. Eckel-Passow, D.H. Lachance, A.M. Molinaro, K.M. Walsh, P.A. Decker, H. Sicotte, M. Pekmezci, T. Rice, M.L. Kosel, I.V. Smirnov, Glioma groups based on 1p/19q, IDH, and TERT promoter mutations in tumors, N. Engl. J. Med. 372 (2015) 2499–2508.
[19] D. Rohle, J. Popovici-Muller, N. Palaskas, S. Turcan, C. Grommes, C. Campos, J. Tsoi, O. Clark, B. Oldrini, E. Komisopoulou, An inhibitor of mutant IDH1 delays growth and promotes differentiation of glioma cells, Science 340 (2013) 626–630.
[20] M. Weller, R. Stupp, G. Reifenberger, A.A. Brandes, M.J. van den Bent, W. Wick, M.E. Hegi, MGMT promoter methylation in malignant gliomas: ready for personalized medicine? Nat. Rev. Neurol. 6 (2010) 39–51.
[21] D.N. Louis, A. Perry, P. Burger, D.W. Ellison, G. Reifenberger, A. Deimling, K. Aldape, D. Brat, V.P. Collins, C. Eberhart, International Society of Neuropathology-Haarlem consensus guidelines for nervous system tumor classification and grading, Brain Pathol. 24 (2014) 429–435.
[22] M. Weller, S.M. Pfister, W. Wick, M.E. Hegi, G. Reifenberger, R. Stupp, Molecular neuro-oncology in clinical practice: a new horizon, Lancet Oncol. 14 (2013) e370–e379.
[23] K. Krapfenbauer, E. Engidawork, N. Cairns, M. Fountoulakis, G. Lubec, Aberrant expression of peroxiredoxin subtypes in neurodegenerative disorders, Brain Res. 967 (2003) 152–160.
[24] R.F. Deighton, T. Le Bihan, S.F. Martin, A.M. Gerth, M. McCulloch, J.M. Edgar, L.E. Kerr, I.R. Whittle, J. McCulloch, Interactions among mitochondrial proteins altered in glioblastoma, J. Neuro-Oncol. 118 (2014) 247–256.
[25] O. Persson, U. Brynnel, F. Levander, B. Widegren, L.G. Salford, M. Krogh, Proteomic expression analysis and comparison of protein and mRNA expression profiles in human malignant gliomas, PROTEOMICS-Clin. Appl. 3 (2009) 83–94.
[26] A.A. Khalil, Biomarker discovery: a proteomic approach for brain cancer profiling, Cancer Sci. 98 (2007) 201–213.
[27] J.-M. Lemée, E. Com, A. Clavreul, T. Avril, V. Quillien, M. De Tayrac, C. Pineau, P. Menei, Proteomic analysis of glioblastomas: what is the best brain control sample? J. Proteome 85 (2013) 165–173.
[28] J. Kalinina, J. Peng, J.C. Ritchie, E.G. Van Meir, Proteomics of gliomas: initial biomarker discovery and evolution of technology, Neuro-Oncology 13 (2011) 926–942.
[29] S.P. Niclou, F. Fack, U. Rajcevic, Glioma proteomics: status and perspectives, J. Proteome 73 (2010) 1823–1838.
[30] S. Khaghani-Razi-Abad, M. Hashemi, M. Pooladi, M. Entezari, E. Kazemi, Proteomics analysis of human oligodendroglioma proteome, Gene 569 (2015) 77–82.
[31] J. Franck, K. Arafah, M. Elayed, D. Bonnel, D. Vergara, A. Jacquet, D. Vinatier, M. Wisztorski, R. Day, I. Fournier, M. Salzet, MALDI imaging mass spectrometry: state of the art technology in clinical proteomics, Mol. Cell. Proteomics 8 (2009) 2023–2033.
[32] D. Bonnel, R. Longuespee, J. Franck, M. Roudbaraki, P. Gosset, R. Day, M. Salzet, I. Fournier, Multivariate analyses for biomarkers hunting and validation through on-tissue bottom-up or in-source decay in MALDI-MSI: application to prostate cancer, Anal. Bioanal. Chem. 401 (2011) 149–165.
[33] M. Wisztorski, B. Fatou, J. Franck, A. Desmons, I. Farre, E. Leblanc, I. Fournier, M. Salzet, Microproteomics by liquid extraction surface analysis: application to FFPE tissue to study the fimbria region of tubo-ovarian cancer, Proteomics Clin. Appl. 7 (2013) 234–240.
[34] J. Quanico, J. Franck, C. Dauly, K. Strupat, J. Dupuy, R. Day, M. Salzet, I. Fournier, M. Wisztorski, Development of liquid microjunction extraction strategy for improving protein identification from tissue sections, J. Proteome 79 (2013) 200–218.
[35] R. Lemaire, D. Wisztorski, M. Hendra, Exploring direct analysis using ionic matrices, Proceedings of 53rd ASMS Conference on Mass Spectrometry, San Antonio, Texas June 5, 2005, p. 9.
[36] H. Thiele, S. Heldmann, D. Trede, J. Strehlow, S. Wirtz, W. Dreher, J. Berger, J. Oetjen, J.H. Kobarg, B. Fischer, P. Maass, 2D and 3D MALDI-imaging: conceptual strategies for visualization and data mining, Biochim. Biophys. Acta 1844 (2014) 117–137.
[37] T. Alexandrov, M. Becker, S.O. Deininger, G. Ernst, L. Wehder, M. Grasmair, F. von Eggeling, H. Thiele, P. Maass, Spatial segmentation of imaging mass spectrometry data with edge-preserving image denoising and clustering, J. Proteome Res. 9 (2010) 6535–6546.
[38] S. Tyanova, T. Temu, A. Carlson, P. Sinitcyn, M. Mann, J. Cox, Visualization of LC-MS/MS proteomics data in MaxQuant, Proteomics 15 (2015) 1453–1456.
[39] J. Cox, M. Mann, MaxQuant enables high peptide identification rates, individualized p.p.b.-range mass accuracies and proteome-wide protein quantification, Nat. Biotechnol. 26 (2008) 1367–1372.
[40] J. Cox, N. Neuhauser, A. Michalski, R.A. Scheltema, J.V. Olsen, M. Mann, Andromeda: a peptide search engine integrated into the MaxQuant environment, J. Proteome Res. 10 (2011) 1794–1805.
[41] C. UniProt, UniProt: a hub for protein information, Nucleic Acids Res. 43 (2015) D204–D212.
[42] B. Vanderperre, J.F. Lucier, C. Bissonnette, J. Motard, G. Tremblay, S. Vanderperre, M. Wisztorski, M. Salzet, F.M. Boisvert, X. Roucou, Direct detection of alternative open reading frames translation products in human significantly expands the proteome, PLoS One 8 (2013), e70698.
[43] J. Cox, M.Y. Hein, C.A. Luber, I. Paron, N. Nagaraj, M. Mann, Accurate proteome-wide label-free quantification by delayed normalization and maximal peptide ratio extraction, termed MaxLFQ, Mol. Cell. Proteomics 13 (2014) 2513–2526.
[44] J.A. Vizcaino, E.W. Deutsch, R. Wang, A. Csordas, F. Reisinger, D. Rios, J.A. Dianes, Z. Sun, T. Farrah, N. Bandeira, P.A. Binz, I. Xenarios, M. Eisenacher, G. Mayer, L. Gatto, A. Campos, R.J. Chalkley, H.J. Kraus, J.P. Albar, S. Martinez-Bartolome, R. Apweiler, G.S. Omenn, L. Martens, A.R. Jones, H. Hermjakob, ProteomeXchange provides globally coordinated proteomics data submission and dissemination, Nat. Biotechnol. 32 (2014) 223–226.
[45] D. Szklarczyk, A. Franceschini, M. Kuhn, M. Simonovic, A. Roth, P. Minguez, T. Doerks, M. Stark, J. Muller, P. Bork, L.J. Jensen, C. von Mering, The STRING database in 2011: functional interaction networks of proteins, globally integrated and scored, Nucleic Acids Res. 39 (2011) D561–D568.
[46] A. Bonnet, S. Lagarrigue, L. Liaubet, C. Robert-Granie, M. Sancristobal, G. Tosser-Klopp, Pathway results from the chicken data set using GOTM, Pathway Studio and Ingenuity softwares, BMC Proc. 3 (Suppl. 4) (2009) S11.
[47] A. Yuryev, E. Kotelnikova, N. Daraselia, Ariadne's ChemEffect and Pathway Studio knowledge base, Expert Opin. Drug Discovery 4 (2009) 1307–1318.
[48] H. Heberle, G.V. Meirelles, F.R. da Silva, G.P. Telles, R. Minghim, InteractiVenn: a web-based tool for the analysis of sets through Venn diagrams, BMC Bioinf. 16 (2015) 169.
[49] T. Bock, H. Moest, U. Omasits, S. Dolski, E. Lundberg, A. Frei, A. Hofmann, D. Bausch-Fluck, A. Jacobs, N. Krayenbuehl, M. Uhlen, R. Aebersold, K. Frei, B. Wollscheid, Proteomic analysis reveals drug accessible cell surface N-glycoproteins of primary and established glioblastoma cell lines, J. Proteome Res. 11 (2012) 4885–4893.
[50] J. Kalinina, J. Peng, J.C. Ritchie, E.G. Van Meir, Proteomics of gliomas: initial biomarker discovery and evolution of technology, Neuro-Oncology 13 (2011) 926–942.
[51] S.P. Niclou, F. Fack, U. Rajcevic, Glioma proteomics: status and perspectives, J. Proteome 73 (2010) 1823–1838.
[52] R. Ait-Belkacem, C. Berenguer, C. Villard, L. Ouafik, D. Figarella-Branger, O. Chinot, D. Lafitte, MALDI imaging and in-source decay for top-down characterization of glioblastoma, Proteomics 14 (2014) 1290–1301.
[53] P. Gautam, S.C. Nair, M.K. Gupta, R. Sharma, R.V. Polisetty, M.S. Uppin, C. Sundaram, A.K. Puligopu, P. Ankathi, A.K. Purohit, G.R. Chandak, H.C. Harsha, R. Sirdeshmukh, Proteins with altered levels in plasma from glioblastoma patients as revealed by iTRAQ-based quantitative proteomic analysis, PLoS One 7 (2012), e46153.
[54] R.V. Polisetty, P. Gautam, M.K. Gupta, R. Sharma, M.S. Uppin, S. Challa, P. Ankathi, A.K. Purohit, D. Renu, H.C. Harsha, A. Pandey, R. Sirdeshmukh, Heterogeneous nuclear ribonucleoproteins and their interactors are a major class of deregulated proteins in anaplastic astrocytoma: a grade III malignant glioma, J. Proteome Res. 12 (2013) 3128–3138.
[55] M.B. Nijaguna, C. Schroder, V. Patil, S.D. Shwetha, A.S. Hegde, B.A. Chandramouli, A. Arivazhagan, V. Santosh, J.D. Hoheisel, K. Somasundaram, Definition of a serum marker panel for glioblastoma discrimination and identification of Interleukin 1beta in the microglial secretome as a novel mediator of endothelial cell survival induced by C-reactive protein, J. Proteome 128 (2015) 251–261.
[56] T. Guo, X. Wang, M. Li, H. Yang, L. Li, F. Peng, X. Zhan, Identification of glioblastoma phosphotyrosine-containing proteins with two-dimensional western blotting and tandem mass spectrometry, Biomed. Res. Int. 2015 (2015) 134050.
[57] P. Simeone, M. Trerotola, A. Urbanella, R. Lattanzio, D. Ciavardelli, F. Di Giuseppe, E. Eleuterio, M. Sulpizio, V. Eusebi, A. Pession, M. Piantelli, S. Alberti, A unique four-hub protein cluster associates to glioblastoma progression, PLoS One 9 (2014), e103030.
[58] M.S. Heroux, M.A. Chesnik, B.D. Halligan, M. Al-Gizawiy, J.M. Connelly, W.M. Mueller, S.D. Rand, E.J. Cochran, P.S. LaViolette, M.G. Malkin, K.M. Schmainda, S.P. Mirza, Comprehensive characterization of glioblastoma tumor tissues for biomarker identification using mass spectrometry-based label-free quantitative proteomics, Physiol. Genomics 46 (2014) 467–481.
[59] R.F. Deighton, T. Le Bihan, S.F. Martin, M.E. Barrios-Llerena, A.M. Gerth, L.E. Kerr, J. McCulloch, I.R. Whittle, The proteomic response in glioblastoma in young patients, J. Neuro-Oncol. 119 (2014) 79–89.
[60] I.D. Popescu, E. Codrici, L. Albulescu, S. Mihai, A.M. Enciu, R. Albulescu, C.P. Tanase, Potential serum biomarkers for glioblastoma diagnostic assessed by proteomic approaches, Proteome Sci. 12 (2014) 47.
[61] V.N. Patel, G. Gokulrangan, S.A. Chowdhury, Y. Chen, A.E. Sloan, M. Koyuturk, J. Barnholtz-Sloan, M.R. Chance, Network signatures of survival in glioblastoma multiforme, PLoS Comput. Biol. 9 (2013), e1003237.
[62] K. Motomura, A. Natsume, R. Watanabe, I. Ito, Y. Kato, H. Momota, R. Nishikawa, K. Mishima, Y. Nakasu, T. Abe, H. Namba, Y. Nakazato, H. Tashiro, I. Takeuchi, T. Mori, T. Wakabayashi, Immunohistochemical analysis-based proteomic subclassification of newly diagnosed glioblastomas, Cancer Sci. 103 (2012) 1871–1879.
[63] R.V. Polisetty, P. Gautam, R. Sharma, H.C. Harsha, S.C. Nair, M.K. Gupta, M.S. Uppin, S. Challa, A.K. Puligopu, P. Ankathi, A.K. Purohit, G.R. Chandak, A. Pandey, R. Sirdeshmukh, LC-MS/MS analysis of differentially expressed glioblastoma membrane proteome reveals altered calcium signaling and other protein groups of regulatory functions, Mol. Cell. Proteomics 11 (2012) (M111 013565).
[64] M. Wisztorski, A. Desmons, J. Quanico, B. Fatou, J.P. Gimeno, J. Franck, M. Salzet, I. Fournier, Spatially-resolved protein surface microsampling from tissue sections using liquid extraction surface analysis, Proteomics (2016).
[65] B. Badie, J.M. Schartner, J. Paul, B.A. Bartley, J. Vorpahl, J.K. Preston, Dexamethasone-induced abolition of the inflammatory response in an experimental glioma model: a flow cytometry study, J. Neurosurg. 93 (2000) 634–639.
[66] D. Hambardzumyan, D.H. Gutmann, H. Kettenmann, The role of microglia and macrophages in glioma maintenance and progression, Nat. Neurosci. 19 (2016) 20–27.
[67] K.M. Lewis, C. Petritsch, Asymmetric cell division: implications for glioma development and treatment, Transl. Neurosci. 4 (2013) 484–503.
[68] W. Roggendorf, S. Strupp, W. Paulus, Distribution and characterization of microglia/macrophages in human brain tumors, Acta Neuropathol. 92 (1996) 288–293.
[69] G.J. Kitange, B.L. Carlson, M.A. Schroeder, P.A. Decker, B.W. Morlan, W. Wu, K.V. Ballman, C. Giannini, J.N. Sarkaria, Expression of CD74 in high grade gliomas: a potential role in temozolomide resistance, J. Neuro-Oncol. 100 (2010) 177–186.
[70] Y.-H. Yu, G.-Y. Chiou, P.-I. Huang, W.-L. Lo, C.-Y. Wang, K.-H. Lu, C.-C. Yu, G. Alterovitz, W.-C. Huang, J.-F. Lo, Network biology of tumor stem-like cells identified a regulatory role of CBX5 in lung cancer, Sci. Rep. 2 (2012).
[71] D.L. Masica, R. Karchin, Correlation of somatic mutation and expression identifies genes important in human glioblastoma progression and survival, Cancer Res. 71 (2011) 4550–4561.

[72] L. Collins, D. Penny, Complex spliceosomal organization ancestral to extant eukaryotes, Mol. Biol. Evol. 22 (2005) 1053–1066.
[73] M. Kretz, Z. Siprashvili, C. Chu, D.E. Webster, A. Zehnder, K. Qu, C.S. Lee, R.J. Flockhart, A.F. Groff, J. Chow, Control of somatic tissue differentiation by the long non-coding RNA TINCR, Nature 493 (2013) 231–235.
[74] Y.B. Beaulieu, C.L. Kleinman, A.-M. Landry-Voyer, J. Majewski, F. Bachand, Polyadenylation-dependent control of long noncoding RNA expression by the poly (A)-binding protein nuclear 1, PLoS Genet. 8 (2012), e1003078.
[75] S. Delic, N. Lottmann, K. Jetschke, G. Reifenberger, M.J. Riemenschneider, Identification and functional validation of CDH11, PCSK6 and SH3GL3 as novel glioma invasion-associated candidate genes, Neuropathol. Appl. Neurobiol. 38 (2012) 201–212.
[76] C.J. Sandberg, E.O. Vik-Mo, J. Behnan, E. Helseth, I.A. Langmoen, Transcriptional profiling of adult neural stem-like cells from the human brain, PLoS One 9 (2014), e114739.